Critical Phenomena of the Ising Model on Triangulations

Masterarbeit aus der Physik

vorgelegt von

Tony Wasserka

15. 01. 2016

Institut für Theoretische Physik
Friedrich-Alexander-Universität Erlangen–Nürnberg

Betreuer:
Prof. Dr. Klaus Mecke
Benedikt Krüger

Contents

1 Introduction

The Ising model has since its original conception in the 1920s [1] by Ernst Ising and especially since its analytical solution [2] by Lars Onsager in 1944 remained an active topic of research and has became one of the most important reference models in statistical physics. Despite being a conceptually simple model, it displays a very rich structure, and is among the simplest physical models that can be solved analytically while being nontrivial enough to exhibit a phase transition [3]. As such, it had a major impact on the development of the theory of phase transitions, critical exponents, and universality. A fairly recent area of interest is a generalized Ising model defined on a graph and, eventually, on random graphs. One of the main questions one can ask in this case is: What universality class does the Ising model on such graphs belong to, and does it behave uniformly across different realizations of the same random graph structure? Some random graphs which have been analyzed within this context are for instance Watts-Strogath networks [4–6] and Barabási-Albert networks [7].

In this thesis, we analyze the Ising model on a graph structure induced by triangulations, the latter which can be used as a mean of discretizing surfaces, volumes, and their higher-dimensional analoga in computational geometry [8], but are not limited to this purpose: In the context of quantum gravity, they are used to describe spin-foams [9] and actually make up the central entities of interest in certain models called *(causal) dynamical triangulations* [10, 11]. The theory of triangulations furthermore finds applications in the treatment of foams, which are commonly described using Voronoi tesselations, which are in a duality relationship to so-called *Delauney triangulations*.

A particular class of triangulations called *lattice triangulations*, which are tesselations of a planar grid with fixed size and fixed vertex coordinates, has been analyzed in terms of their properties as random graphs in [12]. The authors assigned the energy functional (4.3) to each lattice triangulation, which they interpret as a measure of *order*. Using this energy functional, they computed canonical expectation values of common graph observables (vertex degree distribution, clustering coefficient, shortest path length) based on numerical groundwork by Knauf et al [13]. It was found that for inverse temperatures below a negative, quasi-critical temperature α_c (with negative temperatures corresponding to disordered triangulations), many graph observables display small-world behavior, while in the vicinity of α_c, the observations hinted at scale-free behavior. Furthermore, all considered graph observables show a cross-over behavior between negative temperatures and positive temperatures.

Another class of triangulations are *topological triangulations*, which are discretized topological manifolds with fixed number of vertices and which, contrary to lattice triangulations, do not fix any vertex coordinates. Based on the finding that any graph can be embedded into a closed surface with high enough genus, a generic methodology was developed to study complex networks by embedding them as subgraph of some topological triangulation[14]. A key insight of this was that the genus of the embedding surface is a central characteristic that affects local and global properties of the embedded graph. A further application is to use topological triangulations to construct random graphs, an example of which are *random Apollonian networks* [15].

Given this background, this thesis is concerned with the analysis of the phase transition in the Ising model on both lattice triangulations and topological triangulations. To this end, we use a numeric approach based on Monte Carlo methods (Section 2.2) and in particular the Wang-Landau algorithm explained in Section 2.3. We outline a number of common methods to determine critical exponents in Section 3.2 and summarize known results about the Ising model in Section 3.3.

For the former class of lattice triangulations, we elaborately look at what we call the *perfectly ordered triangulation* in Section 4.2.2 and find that its universality class matches the one of the standard 2D Ising model as evident by its critical exponents (cf. Table 3). We furthermore consider random ensembles of lattice triangulations, for which we find a scattered distribution of values of the critical exponents as depicted in Figure 15. Finally, we introduce a canonical ensemble of triangulations with regards to an energy functional (4.3) that describes a notion of *order*. In Figure 17, we show that the critical temperature in this ensemble shows a crossover behavior with regards to the ensemble parameter, with one regime reproducing the results of the perfectly ordered triangulation and the other showing new behavior. The transition point reproduces the behavior of the random ensemble. The observed cross-over behavior can be considered to be an analogy of the previously observed effects on graph observables to the Ising model.

For the latter class of topological triangulations, as shown in Figure 22 we find that depending on the genus g of the triangulated manifold, the quasi-critical inverse temperature obtained from finite-size system simulations may be decreasing ($g = 0$) or increasing ($g > 1$) with the system size, or it may not depend on the system size at all ($g = 1$). We believe this can be explained by an effective increase of the coupling strength due to changes in the ratio of edges to vertices (see Equation (5.10)).

2 Monte Carlo Simulations of Phase Transitions

In this chapter, we will define basic notions of statistical physics, putting particular emphasis on the theory of phase transitions, and lay down the mathematical notation. The reader is assumed to be familiar with the core concepts of these topics, so there will be no in-depth derivations of the results mentioned. We furthermore introduce the idea and concepts of *Markov chain Monte Carlo*, which is the primary method of simulation that we use in this thesis.

2.1 Statistical Physics and Phase Transition Theory

This section will briefly refresh the basic concepts of statistical physics, as described in more depth e.g. in [16–18].

2.1.1 Ensembles, Expectation Values, and Thermodynamic Potentials

Statistical physics is concerned with the analysis of a system by considering ensembles — i.e. a hypothetical infinite amount of different realizations of the same system. The individual copies of the system within such an ensemble will be different in their microscopic details in general, but certain macroscopic quantities will emerge as "common" across the ensemble, within some statistical error. These quantities and their fluctuations are computed by stochastic averages over the ensemble, which is why probability theory is central for statistical physics. Indeed, these averages are determined by how likely individual configurations of the ensemble are to be realized. In the simplest case (called *random ensemble*), all microscopic system states are distributed uniformly within the ensemble. In a *microcanonical ensemble*, only states with a certain energy may be assumed. A third class is the *canonical ensemble*, in which states are distributed according to the Boltzmann factor

$$p_{\text{can}}(\omega) \propto \exp(-E(\omega)/kT) \tag{2.1}$$

with $E(\omega)$ the energy of the considered state ω, k the Boltzmann constant and T the system temperature[1].

All of these ensembles can be described generically using appropriate probability distributions of states within the ensemble, and in fact these distributions can be derived from the fundamental law of statistical physics [19]It is postulated that *a priori* (i.e. based upon the knowledge about the system before measuring any experiment or simulation outcomes), the probability to find the system in any state that fits the given knowledge is equal. Without any knowledge about the system, this predicts a random ensemble, while e.g. an isolated system at a specific energy is best described using a microcanonical ensemble. The Boltzmann distribution (2.1) used for canonical ensembles is predicted when considering systems in thermal equilibrium.

For many ensembles, the probabilities of states is given without normalization. For instance, the Boltzmann factors of all states in a canonical ensemble in general don't add up to 1. For a generic, discrete system with a state space Ω and weighting factors

[1] A common notation is $\beta = \frac{1}{kT}$, such that that equations like (2.1) simplify to $p_{\text{can}}(\omega) \propto \exp(-\beta E(\omega))$.

$\rho(\omega)$ for any $\omega \in \Omega$, the normalization factor is obtained by computing the *partition function*[2]

$$Z = \sum_{\omega \in \Omega} \rho(\omega), \tag{2.2}$$

such that the probability of any state ω is given by

$$p(\omega) = \frac{1}{Z}\rho(\omega). \tag{2.3}$$

More generally, the partition sum is also the normalization factor used to compute ensemble averages of any physical quantity $\mathcal{O}(\omega)$ of the system:

$$\langle \mathcal{O} \rangle_\rho = \sum_{\omega \in \Omega} p(\omega)\mathcal{O}(\omega) = \frac{1}{Z} \sum_{\omega \in \Omega} \rho(\omega)\mathcal{O}(\omega). \tag{2.4}$$

In the following, we will denote expectation values of microcanonical and canonical ensembles as $\langle \mathcal{O} \rangle_{\text{mc}}$ and $\langle \mathcal{O} \rangle_{\text{can}}$, respectively.

All thermodynamic (i.e. macroscopic) state of a system can be completely encoded in *thermodynamic potentials*, i.e. scalar functions which depend only on thermodynamic variables characteristic to the system. Knowledge of the functional dependency of the thermodynamic potential allows recovering all thermodynamic quantities through the use of derivatives of the potential. In particular in a system in equilibrium (with unchanged outer conditions), the corresponding thermodynamic potential always takes a minimum. As an example, in canonical ensembles the thermodynamic potential is the (Helmholtz) free energy[3]

$$F(T, V) = U(T, V) - T \cdot S(T, V) = -kT \log Z(T, V), \tag{2.5}$$

where S is the system entropy and U may be considered the ensemble average of the total system energy, and where the second equality is implied by computing the U through Equation (2.4) and the entropy through Equation (2.3).

Using the free energy, derivatives of the free energy with respect to the system temperature can be used to compute expectation values of the energy, for instance

$$\langle E \rangle_{\text{can}} = \frac{\partial}{\partial \beta}(\beta F) = -\frac{1}{Z}\frac{\partial Z}{\partial \beta} \tag{2.6}$$

and

$$\left\langle E^2 \right\rangle_{\text{can}} = \left(\frac{\partial(\beta F)}{\partial \beta}\right)^2 + \frac{\partial^2(\beta F)}{\partial \beta^2} = -\frac{1}{Z}\frac{\partial^2 Z}{\partial \beta^2}. \tag{2.7}$$

[2] For discrete systems the partition function represents the total number of states. As explained below, this actually encompasses much more information than just a normalization factor: In fact, the partition sum encodes the full thermodynamic state of the system.

[3] In this case, the expression given for the free energy is simplified for the case of a system with fixed particle number.

2.1.2 Theory of Phase Transitions

Many physical systems feature characteristic global structures called *phases*. An example of this phenomenon is H_2O with its liquid (water), gaseous (vapor), and solid (ice) states, but the phase space may be much richer like in the case of metallic alloys like steel, which has a multitude of different phases despite being a system of only two chemical elements. When considering the thermodynamic space of a system, a phase often manifests as an "isle" of states which behave similar in some way.

These isles are well-separated (i.e. there is no crossing of two phases), but the border between two or more phases does describe states of *phase coexistence*. A process which runs through thermodynamic space from one phase across such a border into another phase is called a *phase transition*. Mathematically, a property common to all phase transitions is that some derivatives of the thermodynamic potential assume a discontinuity at the point of phase coexistence. This observation provides the base for defining phase transitions rigorously; The location of the discontinuity is referred to as the *critical point*, and phase transitions are accordingly referred to as *critical phenomena*. Historically, the order of the lowest derivative of the thermodynamic potential at which the discontinuity occurs was often used to denote an *phase transition order*. Today, the classification of phase transitions is more sophisticated [20], but the simplified terminology suffices for this thesis.

Upon analysis of the system behavior close to the critical point, it has been found that phase transitions have a mathematically richer structure, which is not limited to the discontinuity itself but also predicts the system behavior at the vicinity of the critical point. By quantifying the proximity to the critical temperature[4] with $t = \frac{T-T_c}{T_c}$, many system observables in leading order follow a power-law for $t \ll 1$. For instance, the specific heat often assumes the form

$$c = |t|^{-\alpha}, \tag{2.8}$$

and similarly for the system's correlation length

$$\xi = |t|^{-\nu}. \tag{2.9}$$

The values of α and ν are called *critical exponents* and are characteristic to each system.

For many systems, it has been found that the set of critical exponents coincide. One speaks of *universality* of critical exponents, and it essentially predicts that the system behavior around the critical point is entirely determined by a few system properties like dimension and symmetry, but does not depend on microscopic details like particle kind, interaction potential, or system shape. As such, the set of critical exponents describing a system defines a *universality class*, and determining particular values of these in one system allows for drawing conclusions in other systems, too. Formally, universality can be treated theroretically by renormalization group theory [21], which we will not go

[4] The critical temperature is the temperature at the critical point. In a canonical ensemble with unchanging volume and particle number (which we will exclusively be concerned with), the critical temperature is equivalent to the critical point.

into here, however. Instead, a number of practical approaches of determining critical exponents is given in Section 3.2.

An important note has to be made in the context of simulations: Since finite systems always have continuous derivatives which only approximate discontinuity with increasing system size, critical phenomena are strictly speaking only defined on systems of infinite size. This poses a problem for the analysis of phase transitions using simulations, which are naturally restricted to finite size. One must hence must be careful when drawing conclusions about critical phenomena in the infinite system based on analysis of finite ones.

2.2 Markov Chain Monte Carlo Methods

For most nontrivial systems, it is *de facto* impossible to calculate expectation values (2.4) or the partition sum (2.2) (with which the former could be computed using derivatives). This is because the number of states rapidly grows with the system size. For instance, the number of states in the Ising model grows exponentially with respect to the system size — doubling the linear system size quadruples the computational effort hence. For this reason, approximative methods are used, a large part of which fall into the class of *Monte Carlo methods*.

This section will first introduce the basic idea of Monte Carlo simulations and how it relates to Markov chains. Later on, we apply the theory to explain how to generate samples of a system such that all energy levels are distributed equally. A full overview of the topic is given e.g. in [22] and in [23].

2.2.1 Monte Carlo Methods

Monte Carlo methods find broad applications in both mathematical and physical problems. Frankly, the term may be defined [24] as any "use of stochastic techniques to solve [...] a deterministic problem". The first Monte Carlo algorithms were designed in a mathematical context to compute integrals over "poorly-behaved functions and integrals in high-dimensional spaces" [25]. An example is the function

$$\sin^2\left(\frac{1}{x}\right), \tag{2.10}$$

which is bound between 0 and 1, and hence confines some "area", yet it oscillates rapidly as x goes towards 0, making traditional methods of integral evaluation impossible to apply.

In a more physical context, the authors Landau and Binder [23] describe a Monte Carlo method as the simulation of a model for which time dependence does not follow a rigorously deterministic procedure, but instead is a discrete stochastic process described by a sequence of randomly generated numbers. The idea is that by running multiple simulations of the same kind with different sequences of random numbers, each simulation will yield different microscopic results on their own, but there will also be values (e.g. macroscopic observables or time-averages) which agree across all simulations within

some *statistical error*. This error ideally then converges towards zero as the number of total simulations increases. Such simulations successfully describe a large variety of problems in physics, in particular those of many-particle systems, like for example fluid simulations or interdiffusion within metallic alloys.

The particular description of the stochastic process is of central importance to the success of this method. Take a system described by a canonical ensemble. Then any observable $f(\omega)$ of a state ω in the state space Ω has an ensemble average

$$\langle f \rangle_{\text{can}}(\beta) = \frac{1}{Z} \sum_{\omega \in \Omega} \exp(-\beta E(\omega)) f(\omega). \tag{2.11}$$

Naively, one would approximate this sum by generating a large number N of uniformly distributed samples $S \in \Omega^N$, each generated by rolling a uniformly distributed random number for each particle position and momentum component. Expectation values can then be estimated using

$$\langle f \rangle_{\text{can}}(\beta) \approx \frac{1}{Z_S(\beta)} \sum_{\omega \in S} \exp(-\beta E(\omega)) f(\omega), \quad Z_S(\beta) = \sum_{\omega \in S} \exp(-\beta E(\omega)) \tag{2.12}$$

with. This method is known as simple sampling. In practice, it converges very poorly since it usually selects states with little contribution to the partition sum (i.e. their probability within the ensemble is very small) [23]. In other words, parts of the whole state space are sampled, but the most relevant states might only cover a very small subspace of that. Hence, simple sampling requires very large sample sizes to yield satisfactory results.

2.2.2 Importance Sampling

Quite often, the systems that perform poorly using simple sampling are characterized by an ensemble probability distribution for which only a small part of the full state space takes a non-negligible value. In particular, this applies to all canonical ensembles, for which the Boltzmann factor (being proportional to an exponential function of the energy) weighs states with small energy more than those with large energy. To improve the convergence behavior for such systems, one modifies the sampling algorithm to sample specific kinds of states (e.g. low-energy states) more often than others. This approach is called importance sampling.

When states are not sampled with equal probability, Equation (2.12) needs to be modified to consider the non-uniform sampling probability. For a generic ensemble of (discrete) states distributed with probability $P(\omega)$, we have the sum

$$\langle f \rangle = \sum_{\omega \in \Omega} f(\omega) P(\omega). \tag{2.13}$$

When given a sequence S of samples which were drawn with a *sampling probability distribution* $P_{\text{samp}}(\omega)$, we now have the estimate

$$\langle f \rangle \approx \frac{1}{N} \sum_{\omega \in S} f(\omega) P(\omega) P_{\text{samp}}^{-1}(\omega). \tag{2.14}$$

The additional division by P_{samp} compared to Equation (2.12) is used to compensate for the fact that some states are sampled more often than others.

The sampling distribution $P_{\text{samp}}(\omega)$ is up to the programmer's choice: Of course, simple sampling emerges by using a uniform distribution, while any non-uniform distribution can be used to weigh "important" states appropriately. A common choice for canonical ensembles is $P_{\text{samp}}(\omega) = P(\omega) = \frac{1}{Z}\exp(-\beta E(\omega))$ (as used e.g. in the Metropolis algorithm), which makes the two probability terms in Equation (2.14) cancel out so that $\langle f \rangle$ is just the average of the sampled states. Note that this example of P_{samp} includes a dependency on the (*a priori* unknown) partition sum, which however need not be a problem; a proper choice of the sampling algorithm (e.g. using Markov chains, as explained in Section 2.2.3) can draw samples following the probability P_{samp} without any knowledge of Z.

2.2.3 Markov Chains and the Metropolis Algorithm

While the theory of importance sampling explains how one can weight states with large contribution towards the partition sum more than those with little contribution, it does not directly provide a way to generate samples with the desired probability distribution. Furthermore, the sampling probability used in Equation (2.14) technically may depend on the partition sum[5], which is of course not known in advance. Many techniques used to resolve these two issues (in particular, the popular Metropolis algorithm) involve the use of *Markov chains*. In the following, we describe what Markov chains are and how they involve stochastic processes, and then describe how they are used to sample states with a given probability distribution.

Markov chains are sequences of states, each of which is generated in a stochastic manner such that the probability for the next state in the chain is solely determined by the current state. In other words, a Markov chain models a process of discrete time which has no memory about any history beyond its current state. There hence is a *transition probability* $P(\omega_i \to \omega_j)$, which describes the probability for the current state ω_i to be followed by ω_j. This probability technically may change with "time" (i.e. the position of ω_i within the Markov chain), but for our purposes we assume time-independent transition probabilities and hence don't denote any time dependence. For particular types of transition processes, as the Markov chain length increases towards infinity there will be a *limiting distribution*

$$P(\omega_i) = \lim_{n\to\infty} \frac{\text{Number of occurrences of } \omega_i \text{ in } M|_n}{n}, \tag{2.15}$$

with $M|_n$ the subsequence of the first n Markov chain elements. In other words, $P(\omega_i)$ is the probability of the state ω_i to be attained as an element within the Markov chain. Markov chains for which such a limiting distribution exists are called *stationary*, and we will in fact only consider stationary Markov chains within in this thesis. Hence, we

[5] In particular, this is the case when the sampling probability is chosen to be proportional to the Boltzmann factor 2.1

can say that the choice of the stochastic process entirely determines the distributions of states within the generated sequence.

The fact that Markov chains have a limiting distribution $P(\omega)$ is the reason why Markov chains can be used to model the dynamics of states in a statistical ensemble distributed according to $P(\omega)$. They may also be used to randomly generate generate realizations of an ensemble with the same probability. In both cases, one usually knows $P(\omega)$ in advance and tries to find $P(\omega_i \to \omega_j)$ which has $P(\omega)$ as its limiting distribution. However, finding a limit-free mathematical connection between $P(\omega_i \to \omega_j)$ and $P(\omega_i)$ is nontrivial in the general case. When describing systems using stationary Markov chains, a natural constraint makes this more straightforward: We demand that the probability of the system to *leave a state* ω_i be equal to the probability of the system to *enter the state* ω_i. Mathematically, this imposes the equation

$$\sum_{\omega_j} P(\omega_i) \cdot P(\omega_i \to \omega_j) = \sum_{\omega_j} P(\omega_j) \cdot P(\omega_j \to \omega_i). \tag{2.16}$$

This equation is known as the *balance condition*. Note that the sums are needed to consider all possible initial and final states, respectively. In practice, one often demands an even stronger property, saying that the probability to *leave state* ω_i *and go to* ω_j is equal to the probability of a transition in the inverse direction, i.e.

$$P(\omega_i) \cdot P(\omega_i \to \omega_j) = P(\omega_j) \cdot P(\omega_j \to \omega_i). \tag{2.17}$$

A physical argument for demanding this equation to hold is that it prevents state transitions that run in "circles" to be sampled, which is desirable because in most real systems such transitions would not be observed. Equation (2.17) is known as *detailed balance*, because it holds for every term within the sums in the balance condition 2.16. Detailed balance provides a very clear connection between *transition probabilities* and *state sampling probabilities*.

Even when imposing detailed balance, there may still be many possible choices for the state transition process. It depends on the considered system which one is applied. For the purpose of this thesis, we split the transition process in two substeps, one being the selection of a potential successor state and the other being the rolling of a random number to determine whether to accept this state as the new Markov chain element or not. This split allows for intuitive algorithms, in which the selection step could for instance be implemented as a simple geometric transformation (for instance, inserting or removing edges in a graph), and where the acceptance probability then is chosen such that the detailed balance condition is met. In particular, the procedure we follow is then as follows:

1. Pick some arbitrary state ω_0 to start with
2. Denote the current state as ω_i
3. Select a random state ω_j using the selection probability $P_S(\omega_i \to \omega_j)$

4. Roll a number to determine whether to accept the selected state as the new state or not (using the acceptance probability $P_A(\omega_i \to \omega_j)$). If the selected state is not accepted, continue using the current state.

5. Append the current state to the Markov chain

6. Repeat at point 2 until a sufficient number of states have been sampled

In summary, each Markov chain element is generated starting from the previous state and then considering a number of state transitions. Essentially, this procedure is a generalization of the Metropolis-Hastings-algorithm.

2.2.4 Flat Histogram Sampling

As mentioned in Section 2.2.2, when performing importance sampling within canonical ensembles one commonly chooses the sampling probability to be proportional to the Boltzmann factor 2.1. When sampling using a Markov chain, detailed balance (2.17) implies that the state transition probability $P(\omega_i \to \omega_j)$ obey the condition

$$P(\omega_i \to \omega_j) = \exp(-\beta(E(\omega_j) - E(\omega_i))) \cdot P(\omega_j \to \omega_i). \tag{2.18}$$

This means that if ω_i is a state of lower energy than ω_j, it becomes increasingly unlikely for a transition from ω_i to ω_j to happen compared to transitions in the opposite direction. This makes it likely to fall into local minima temporarily. However, when using the Metropolis-Hastings-algorithm, considered transitions are usually between states which are connected through a "simple" geometry transformation. Hence if the current state is a local energy minimum, there is a danger that the global minimum is located elsewhere, and that we thus do not sample from the whole relevant state space. This is especially relevant in systems with continuous phase transitions.

An approach to resolve this is to use a different kind of importance sampling called *flat-histogram sampling*, in which the sampling weights are chosen such that all system energy levels have equal probability to have a state of the corresponding energy to be sampled. As such, sampling will not get stuck in energy minima by design. The name refers to the flat incidence histogram obtained by counting the number of states sampled from each of the energy levels. The algorithm requires knowledge of a quantity called *density of states*, which is a function g mapping an energy E to the number of states with that energy, i.e.

$$g(E) = \sum_{\omega \in \Omega} \delta(E - E(\omega)). \tag{2.19}$$

Computing this function is a highly nontrivial task, but we show an algorithm to compute it in Section 2.3 and for now assume it's known. The sampling algorithm is called *flat-histogram sampling* and is implemented by choosing $P_S(\omega) = (g(E(\omega)))^{-1}$. Equation (2.14) implies the estimator

$$\hat{f} \approx \frac{1}{|S|} \sum_{\omega \in S} f(\omega) P(\omega) g(E(\omega)). \tag{2.20}$$

for an observable f of an ensemble with state distribution $P(\omega)$.

In a canonical ensemble, $P(\omega)$ purely depends on the state through its energy. For such ensemble distributions, flat-histogram sampling and an analytic identity allow for further simplification of Equation (2.20). Writing $P(\omega) = P(E(\omega))$ by abuse of notation, we analytically have

$$\begin{aligned}\langle f\rangle_{\text{can}} &= \sum_{\omega\in\Omega} P(E(\omega))f(\omega) = \sum_{E}\sum_{\omega\in\Omega} P(E)\delta(E-E(\omega))f(\omega)\\ &= \sum_{E} P(E)\underbrace{\sum_{\omega\in\Omega}\delta(E-E(\omega))f(\omega)}_{=g(E)\cdot\langle f\rangle_{\text{mc}}(E)} = \sum_{E} P(E)g(E)\langle f\rangle_{\text{mc}}(E). \end{aligned} \tag{2.21}$$

In this equation, $\langle f\rangle_{\text{mc}}(E)$ is the average value of all states with energy E. We can see that the sum over all system states is replaced by a sum over all system energies, which makes a tremendous difference for many systems. For instance in an Ising model with V spins, the number of states is 2^V (i.e. it scales exponentially with the system size) while the number of energy levels increases linearly in V. Arguably, the "missing" sum terms are hidden in $\langle f\rangle_{\text{mc}}(E)$, but since that expression does not depend on any additional parameters (e.g. the system temperature β), it can be estimated once so that any changes to β only need to have the sum over energy levels re-evaluated. To estimate $\langle f\rangle_{\text{mc}}(E)$, we restrict the sample sequence S to the subsequence $S'(E)$ of states with energy E (all of which have equal probability to be sampled), applying Equation (2.14) yields the estimator

$$\begin{aligned}\langle f\rangle_{\text{mc}} &= \frac{1}{g(E)}\sum_{\omega\in\Omega} f(\omega)\delta(E-E(\omega)) \approx \frac{1}{g(E)}\frac{1}{|S'(E)|}\sum_{\omega\in S'(E)} f(\omega)\delta(E-E(\omega))\underbrace{P_S^{-1}(\omega)}_{=g(E)}\\ &= \frac{1}{|S'(E)|}\sum_{\omega\in S'(E)}\delta(E-E(\omega))f(\omega). \end{aligned} \tag{2.22}$$

So in other words, $\langle f\rangle_{\text{mc}}(E)$ may be considered to be an expectation value in the micro-canonical subensemble of states with energy E.

2.3 The Wang-Landau Algorithm

We now turn our attention to the Wang-Landau algorithm, which is a method to compute the density of states $g(E)$ used for flat-histogram sampling. We first outline the idea and method of the algorithm as presented originally [26]. We then go into more detail about our particular implementation, which adds a few optimizations to improve the convergence behavior for our particular scenario.

2.3.1 High-Level Description

The defining characteristic of flat-histogram sampling is that counting the number of times each energy level of the system is visited in the Markov chain will yield an equal

amount of visits for each energy. This relies on the assumption that the density of states $g(E)$ is precisely known; if instead a Markov chain is constructed using the transition probability from flat-histogram sampling $\left(P(\omega_i \to \omega_j) = \min\left(\frac{\tilde{g}(E(\omega_i))}{\tilde{g}(E(\omega_j))}, 1\right)\right)$ using an *estimate* $\tilde{g}(E)$, some energies will be sampled more often than others. We can find a more accurate estimate by increasing our estimate for $g(E(\omega_j))$ whenever a state ω_j is visited during sampling. This will decrease the ratio $\frac{\tilde{g}(E(\omega_i))}{\tilde{g}(E(\omega_j))}$, and hence a future step to $E(\omega_j)$ from any other energy level will be less likely. Energy levels which are visited too frequently initially will thus be sampled with more balance as the number of samples drawn increases.

More precisely, the algorithm is initialized by setting our estimate $\tilde{g}(E) = 1$ for all energy levels, since *a priori* we have no information about it. We then proceed by picking some initial state of the system, from which a random walk between system states is started using the transition probability[6] $P(\omega_i \to \omega_j)$. After each step of the random walk, the estimate of the density of states of the current state's energy is replaced by its current value multiplied by a *modification factor* $f > 1$, i.e. $\tilde{g}(E) \to f \cdot \tilde{g}(E) > \tilde{g}(E)$. During the random walk, we also record a histogram the number of times each energy level is visited. The convergence speed of the simulation largely depends on the initial choice of the modification factor: Large choices will speed up the computation, but imply greater statistical errors, while small values increase the time the random walk needs to reach all relevant states. A conservative choice for the initial value of f is Euler's number, i.e. $f = 2.71828$.

After each 10000 steps[7], we check whether the density of states approximates a flat walk in energy space yet. Note that by strict definitions of "flat", the algorithm will not converge in practical time. Instead, we consider the histogram to be "flat enough" if no energy level has been visited less than the histogram average times some fixed percentage p. Choosing p close to 100% is equivalent to demanding a perfectly flat histogram, while values less than that allow small bumps to be present. We use a fairly conservative value in the range of $80 - 90\%$.

If the histogram is not considered flat, we continue the random walk and check again after 10000 steps. Once it is flat, the current estimate $\tilde{g}(E)$ is assumed to be reasonably close to the true value. To improve the estimate further, we reset the histogram to zero and repeat the procedure using a smaller modification factor f to allow for fine-grained adjustments on the the estimate $\tilde{g}(E)$. In particular, we set $f \to f^n$, with n some constant less than 1 (we use $n = 0.9$). The remaining deviation of $\tilde{g}(E)$ to the true density of states is proportional to $\log(f)$ and as such converges to zero. We stop the computation as soon as f assumes a value lower than a particular threshold (in our case, $f < 1.00001$ as will be justified in Section 4.2.1).

[6] Note that the there may be a non-zero probability for the random walk to stay in the current state

[7] Any other number could be chosen, but 10000 is sufficient to yield acceptable runtime performance.

2.3.2 Technical Implementation Details

There are a number of additional measures one can take to compensate for a number of weaknesses in the algorithm.

One major point is that the Wang-Landau algorithm only obtains a density of states *proportional* to the true function. This is sufficient for applications which only make use of *ratios* of the density of states between two energy levels (e.g. flat-histogram sampling, or the computation of expectation values). However, normalizing the estimate regardless is beneficial for two reasons:

- to make sure the value of $g(E)$ does not grow beyond an amount that can be stored in a double-precision floating point value[8]
- to make sure the density of states resulting from multiple Wang-Landau runs (with multiple random number seeds) are comparable against each other. This is relevant for determining errors.

If the number of states is analytically known for some energy level E_0 (which is the case for the Ising model), we normalize our estimate correspondingly: For a density of states stored as a logarithmic table, this can easily be done via

$$\ln \tilde{g}(E) = \ln \tilde{g}_{raw}(E) - \ln \tilde{g}_{raw}(E_0) + \ln\left(g(E_0)\right), \tag{2.23}$$

for each energy E, and with $\tilde{g}_{raw}$ the output of the Wang-Landau-algorithm and $g(E_0)$ the known number of states. We repeatedly perform this normalization every 1000 iterations during the Wang-Landau algorithm. We furthermore normalize whenever the flatness check succeeds.

Another adjustment to the original algorithm that we made is resetting the incidence histogram $H(E)$ after a certain number of iterations: In the very beginning of the simulation, $g(E)$ is set to 0 and hence a completely (unweighed) random walk is performed (i.e. the transition probability for any considered state change will be 1). As such, the histogram built in the very beginning may look vastly different from what one would get when starting with a more educated guess for the density of states. Hence, we clear the incidence histogram to zero after 100000 iterations times the system size.

A final note is specific to a property of Ising systems, for which the high-energy levels with negligibly small values of the density of states (in relation to states of slightly lower energy). Considering the state transition probability for flat-histogram sampling, it hence becomes very unlikely to find a state transition which moves to that state, and furthermore the acceptance probability to switch away from the high-energy level becomes very small. These two effects make it very hard to obtain a flat incidence histogram. Since these energy levels contribute very little to the final result anyway, we hence introduce an energy cutoff, which automatically rejects Markov chain transitions

[8] Note that technically, we store $g(E)$ as a logarithmic quantity, however it is necessary to expand it to a non-logarithmic one when computing expectation values (see Equation (2.21)). Even when using arbitrary-precision arithmetic, we have found it to be beneficial to have a bound on the computations for performance reasons.

when they yield an energy state higher or equal to the cutoff. This cutoff could for instance be chosen to be $E_{\text{cutoff}} = c \cdot \langle E \rangle$ with $c > 1.0$ some constant and $\langle E \rangle$ the mean system energy, which one could obtain by running a Metropolis simulation of the system at temperature $\beta = 0$.

We went for a more complicated approach, which instead adjusts an "optimal" cutoff dynamically. Initially, the cutoff is set to $+\infty$, and then reduced whenever the following conditions are met:

- the flatness check succeeds for the whole histogram without the highest energy level E_{high} below the cutoff
- the difference between $\tilde{g}(E_{\text{high}}$ and $\tilde{g}(E_{\text{below}}$, where E_{below} is the highest energy level below E_{high}, is larger than the fixed threshold 100
- the incidence histogram value $H(E_{\text{high}})$ is at least 100 times larger than $H(E_{\text{below}})$, since otherwise we might decrease the energy levels too rashly

In any case, it should be noted that this workaround restricts us to the analysis of ferromagnetic Ising models, since in anti-ferromagnetic models, the highest-energy levels have a very noticeable impact on system behavior.

3 The Ising Model on complex Networks

The Ising model, originally developed as an attempt to describe ferromagnetism [1], has established itself as the most popular reference model in statistical physics and the physics community has developed a multitude of different variations and generalizations of the original model. One reason for the interest in the Ising model is that many of its variants are simple enough to be solved analytically, yet exhibits non-trivial effects like phase transitions. Indeed, the study of phase transitions in the various modifications of the Ising model has become an area of ongoing research. This thesis is concerned with a variant of the model which is defined on generic graphs rather than a square lattice. In particular, we will consider *triangulations* (cf. Sections 4 and 5) as the base graph of the model.

This section will first introduce the notation of the generalized Ising model along with common quantities of interest. We then present the numeric methods that we use for analyzing critical phenomena, and finally provide a summary of prior results on commonly used graphs. Throughout this section, the reader is assumed to be familiar with the standard Ising model and effects observed within.

3.1 Definition and Terminology

We consider the Ising model living on a generic[9] graph G with a set of vertices V and edges $E \subset V \times V$ connecting two vertices. The model assigns a *spin* σ_v taking the values $+1$ or -1 to each vertex v. Clearly, the state space Ω of the general system consists of all possible assignments of these values to any of the vertices on the graph, i.e.

$$\Omega = \{\{\sigma_i\}_{i\in V} | \sigma_k \in \{-1, +1\} \forall k \in V\}\,. \tag{3.1}$$

Edges represent interaction between the two spins of the connected vertices, which may be attractive or repulsive. Mathematically, this is realized by introducing an *energy functional*

$$E = -J \sum_{(i,j)\in E} \sigma_i \sigma_j, \tag{3.2}$$

where J is the *coupling constant*, which specifies the interaction strength. Positive values for J correspond to ferromagnetic models, in which spins lower the energy if they have the same value and increase it otherwise, while negative values describe anti-ferromagnetic models, for which the inverse effects on the energy hold. Throughout this thesis, we focus our attention to ferromagnetic models. Using the energy functional (3.2), one can easily define a canonical ensemble of Ising states and perform statistical physics on it.

It is clear how this description generalizes the standard Ising model living on an N-dimensional lattice, which can be considered to be a graph with the lattice sites as vertices, with each neighboring pair of vertices connected by an edge. Note that the notion of periodic boundary conditions cannot be uniquely generalized, however in the

[9] For simplicity, we assume the graph to be connected and note that all explanations extend trivially to disconnected graphs.

case when there is an embedding of the graph into some Euclidian space (yielding e.g. a grid-like structure), there may be an intuitive way to do so by inserting additional edges between pairs of the outermost vertices. In particular we will do this for the perfectly ordered lattice triangulation which we introduce in Section 4 and the border of which is the same as for square lattices.

It is easy to see that (in analogy to the regular Ising model) a spin configuration in which all spins have the same value represents the ground state with regards to the energy functional 3.2. This ground state is twice degenerate, since there are exactly two values the spins may take. The highest-energy state of regular Ising models (characterized by alternating spin directions) has no simple generalization for a generic network topology.

In canonical ensembles of spin configurations, some observables of interest are the specific heat

$$c = -\frac{k\beta^2}{|V|}\mathrm{Var}(E), \tag{3.3}$$

the canonical expectation value $\langle m \rangle_{\mathrm{can}}$ of the (spontaneous) magnetization

$$m = \frac{1}{|V|}\left|\sum_{v\in V}\sigma_v\right|, \tag{3.4}$$

and the magnetic susceptibility

$$\chi = \frac{\beta}{|V|}\mathrm{Var}\left(\sum_{v\in V}\sigma_v\right). \tag{3.5}$$

It is well-known that in the thermodynamic limit of the standard 2D Ising model (see Section 3.3.1), there is a second order phase transition at a critical temperature β_c. In the vicinity of β_c, the theory of critical phenomena (cf. Section 2.1.2) predicts the observables m, χ, and c to be described by a power law with respect to the reduced temperature $t = \frac{\beta_c - \beta}{\beta}$. In particular, we have:

$$\xi \propto t^{-\nu} \qquad c \propto t^{-\alpha} \qquad m \propto t^{\beta} \qquad \chi \propto t^{-\gamma} \tag{3.6}$$

Interestingly, we can insert the expression for ξ into the other equations and obtain:

$$c \propto \xi^{\frac{\alpha}{\nu}} \qquad m \propto \xi^{-\frac{\beta}{\nu}} \qquad \chi \propto \xi^{\frac{\gamma}{\nu}} \tag{3.7}$$

3.2 Determination of Critical Exponents

Determining critical exponents of the generalized Ising model analytically is a highly nontrivial task. A common method is the Bethe-Peierls approach [27, 28], which is exact only for a small class of graphs (see below) but often is a good approximation [29]. Other approaches are the replica trick and the cavity method [30] .

Usually, these methods rely on particular properties of the network structure, and hence may not be applicable generally. We instead use established numerical methods as explained in the following. For details, refer to [31].

3.2.1 Finite Size Scaling

One consequence of this is that these systems have the correlation length as their only *characteristic length scale* in the sense that all scaling laws near the critical point can be rewritten in terms of this length scale, e.g.

$$c = |\xi|^{\alpha/\nu}. \tag{3.8}$$

This observation is important for practically estimating critical exponents in simulations of finite systems, as explained in Section 3.2.1.

Finite-size-scaling (*FSS*) refers to a method used to generalize the power-laws in Equation (3.6), which only hold in the thermodynamic limit, to finite systems: The core FSS hypothesis [32] is based on the observation that the only characteristic length scale of thermodynamic systems at their critical point is the correlation length ξ, which diverges when approaching the critical point. For finite systems, it is clear however that the correlation length cannot become greater than the linear system size L. Hence, it is assumed that the scaling laws (3.7) expressed in terms of the correlation length remain valid in finite systems when considering ξ to be equal to L. This yields the *FSS relations* which hold for the infinite system in the vicinity of the critical temperature T_c. For systems of finite size, we expect the linear system size L to dominate the correlation length ξ. Hence we have the finite-size scaling (FSS) ansätze

$$\langle m \rangle_{\text{can}}(\beta_{c,I}) \propto L^{-\beta/\nu} \tag{3.9}$$

and

$$\chi(\beta_{c,I}) \propto L^{\gamma/\nu}. \tag{3.10}$$

These relations can be used to estimate the values of β/ν and γ/ν by fitting a power-law to the values of $\langle m \rangle_{\text{can}}(\beta_{c,I})$ and $\chi(\beta_{c,I})$ for different system sizes L. In fact [33], the FSS ansätze hold even for temperatures slightly off the true critical temperature $\beta_{c,I}$, and hence the estimate can be done even when only an estimate for the true critical temperature is known. A good estimate is the temperature which maximizes the magnetic susceptibility, since that is the location of the phase transition in the infinite-size limit.

There are some limitations to FSS: First of all, it provides no direct way of estimating the critical exponent ν, and hence estimates for the fractions β/ν and γ/ν can only provide insight into the other critical exponents when ν is obtained through other means (see Section 3.2.2). Furthermore, Equations (3.9) and (3.10) only hold if the dominant behavior around the critical temperature indeed is described by a power law; there may however be systems with critical exponents equal to zero, in which logarithmic corrections need to be included for the FSS ansätze to be applicable. Hence, while some of these effects can be alleviated by including (analytically or empirically determined) corrections, it may not always clear whether FSS leads to useful results or not.

A similar issue arises when the examined system does exhibits strong boundary effects (e.g. due to non-periodic boundary conditions), since these effects may be of similar magnitude as the exponential terms, especially for small system sizes. To illustrate this,

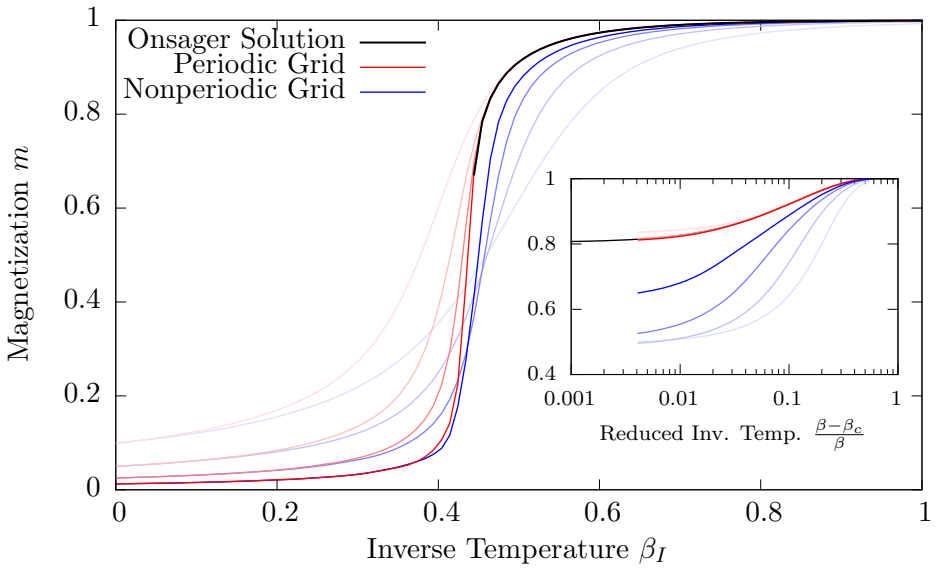

Figure 1: Dependence of the magnetization on the inverse temperature for different lattice sizes (L=8,16,32,64) and different boundary conditions. Inset: Vicinity of the critical point. While the Ising model on a periodic lattice agrees well with the analytic Onsager solution even for small (L≥16) lattices, a free lattice shows strong deviations from the critical behavior even for $L = 64$.

we analyze the regular 2D Ising model on a square-lattice, once with periodic boundary conditions and once with open boundary conditions. The analysis is performed using the Wang-Landau-algorithm (cf. Section 2.3) and flat histogram sampling (cf. Section 2.2.4), through which we obtain estimates for any system observable at any particular system temperature. Comparing the magnetization Figure 1 for both boundary conditions against the analytic solution by Onsager (cf. Section 3.3.1) shows that periodic boundaries yield a behavior close to the analytic solution even for small lattice sizes, while open boundaries require comparatively large system sizes ($L \geq 64$) to get close to the analytic solution.

3.2.2 Binder Cumulant Method

An issue with the method for determining critical exponents outlined in Section 3.2.1 is that the maximal values of observables do not strictly follow the FSS laws (3.9) and (3.10), but have lower-order finite-size dependencies, which need to be taken into consideration for small system sizes ($L < 1000$). Furthermore, finite-size scaling does not directly allow for determining the critical exponent ν of the correlation length ξ.

A method which often yields better results, originally used by Binder [34], is to consider

the *Binder cumulant*, which is defined as

$$U_L = 1 - \frac{\langle m^4 \rangle_{\text{can}}}{3 \langle m^2 \rangle_{\text{can}}^2}. \tag{3.11}$$

The expectation values are taken with respect to the canonical ensemble of Ising states, hence the Binder cumulant is a function of the ensemble temperature β_I. $U_L(\beta_I)$ is a monotonous function, with the high- and low-temperature limits 0 and $\frac{2}{3}$, respectively[10]. These limits do not depend on the linear system size L. A remarkable observation is that in the thermodynamic limit, the value U_L^* of the Binder cumulant at the critical temperature is "universal" within certain classes of systems. These properties are shown in Figure 2.

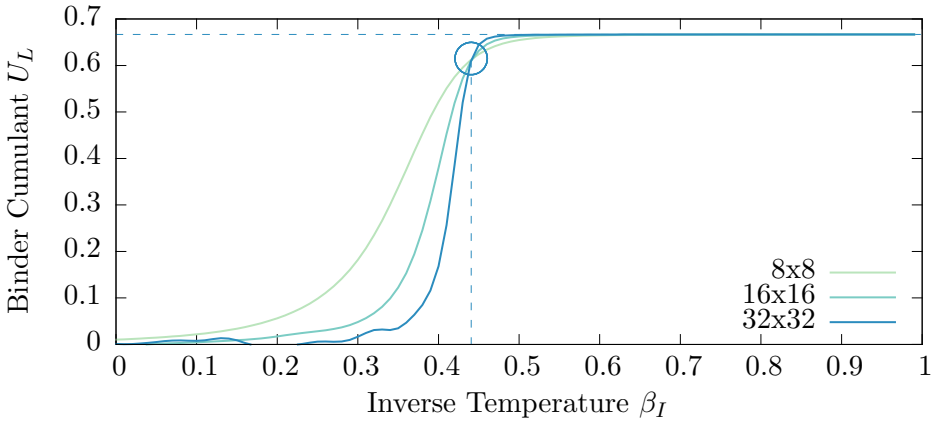

Figure 2: Comparison of the Binder cumulant across different system sizes for the square-lattice Ising model with periodic boundaries: The pairwise intersection points of the three curves are used to estimate the critical temperature in the thermodynamic limit. Despite the comparatively small system sizes, a single intersection point is well-determined. Note that the bumpiness in the plot for the 32x32 lattice is due to the relatively small number of 1000 flat-histogram samples per energy level (compared to 4000 and 16000 for the 16x16 and 8x8 systems, respectively).

It has been found that in many cases, even finite systems agree well on the value U_L^* at the critical temperature. This allows for using the Binder cumulant for estimating the critical temperature: U_L is evaluated on a range of values of β and for different system sizes L_i. Then, one finds the pairwise intersection of the $U_L(\beta_I)$ graphs with regards to ascending pairs of system sizes (i.e. L_1/L_2, L_2/L_3, ...). With increasing system sizes, the intersection points should tend towards the critical temperature of the system. The final estimate can be obtained through extrapolation or by using the intersection point of the largest two systems available.

[10]This can be seen by considering the properties of the ordered and disordered phases: $\lim_{\beta_I \to \infty} \langle |m|^n \rangle_{\text{can}} = 1$ and $\lim_{\beta_I \to 0} \langle |m|^n \rangle_{\text{can}} \to 0$.

By considering the derivative with respect to the inverse temperature β_I, it can be seen that the Binder cumulant encodes further information beyond the critical temperature. Indeed, comparing the value of this derivative at the critical temperature $\beta_{c,I}$ across different system sizes L yields the equation

$$\left.\frac{\partial U_L}{\partial \beta_I}\right|_{\beta_{c,I}} \propto L^{1/\nu}. \tag{3.12}$$

Assuming this equation holds rigorously, one can estimate ν through a power-law fit to Equation (3.12).

While the resulting values are still dependent on the system size, they often are much less relevant than for other methods. However, it should be noted that the universality of U_L^* is not necessarily given for any kind of network structure. In fact, U_L^* itself depends on a number of factors, including boundary conditions and anisotropy [35, 36] of the underlying network. Hence it may happen that the compared Binder cumulant graphs do no intersect in a common point at all. Equation (3.12) also need not hold rigorously. As such, care must be taken when using the Binder cumulant to estimate the critical temperature or critical exponents.

3.3 Known Results for specific Graphs

The main subject of this thesis is the analysis of the universality class of the Ising model on triangulations, which can be interpreted as graphs constituted by many short-loops. To provide a base of reference, we introduce a number of reference models in this section, along with known results on their critical behavior. These results are summarized in Table 1, with more detailed explanations on the derivation of these results as well as notation used therein following after. Note that the table omits the critical exponent ν of the correlation length, since there is no direct way of defining this observable on generic graphs.

Table 1: List of Ising-like models exposing phase transitions with known critical exponents. Entries marked with a dash are values that we have not found any prior results for.

Type	α	β	γ	ν
2D square lattice	0	1/8	7/4	1
3D cubic lattice (approx.)	0.1096(5)	0.32653(10)	1.2373(2)	0.03639(15)
Mean field	0	$\frac{1}{2}$	1	–
Bethe lattices, Cayley trees	0	$\frac{1}{2}$	1	–
Scale-free with $\tau \in (2,3)$	$(\tau-1)/(3-\tau)$	$1/(\tau-3)$	1	–
Scale-free with $\tau \in (3,5)$	$(\tau-5)/(\tau-3)$	$1/(\tau-3)$	1	–
Scale-free with $\tau > 5$	–	1/2	1	–

3.3.1 Cartesian Grid

Cartesian grid are the kinds of "graphs" on which the Ising model has historically drawn the most attention initially. The one-dimensional case, i.e. an infinite chain of spins interacting with their neighbors each, was solved analytically in Ising's thesis [1]. A key insight of the solution is that the system's free energy is an analytic function, and hence the system exhibits no phase transition.

While conceptually very similar to the one-dimensional model, the two-dimensional *square lattice* model hadn't been analytically solved until 1944 by Lars Onsager [2]. In particular, the analytic solution predicts an integral expression for the free energy per site [37],

$$f = -\frac{1}{2\pi\beta_I} \int_0^\pi \ln\left(2\left(\cosh 2\beta_I J\right)^2 + 2k^{-1}\left(1 + k^2 - 2k\cos 2\theta\right)^{\frac{1}{2}}\right) \mathrm{d}\theta \tag{3.13}$$

with

$$k = \left(\sinh 2\beta_I J\right)^{-2}. \tag{3.14}$$

A consequence of Equation (3.13) is that the square lattice Ising model has a second-order phase transition, which can be seen by ignoring all analytic terms of the original equation and expanding remaining parts in terms of their dominant behavior[11]. This yields the *singular part* f_s of the free energy

$$f_s = -\frac{(1+k)(1-k)^2}{2\pi\beta_I k\left(\cosh 2\beta_I J\right)^2} \ln\left|\frac{1+k}{1-k}\right|. \tag{3.15}$$

Clearly, this function (and hence f itself) has a single singularity for $k = 1$. This means that the 2D square lattice Ising model has exactly one critical temperature $\beta_{c,I}$, defined through

$$\sinh\left(2\beta_{c,I} J\right) = 1 \Leftrightarrow \beta_{c,I} = \frac{\ln\left(1+\sqrt{2}\right)}{2J}. \tag{3.16}$$

Knowledge of the free energy allows for deriving all system observables and their critical exponents. For instance, the spontaneous magnetization is predicted [38] to take the form

$$M = \left(1 - \left(\sinh\left(2\beta_I J\right)\right)^{-4}\right)^{\frac{1}{8}} \tag{3.17}$$

for $\beta_I > \beta_{c,I}$. For $\beta_I \leq \beta_{c,I}$, M is identically zero. To obtain the critical exponent β, we expand Equation (3.17) in terms of the reduced temperature $t = \frac{T - T_C}{T_C}$, for which around the critical point we have $t \ll 1$. Expanding the sinh argument to first order in

[11] For details, refer to [37].

t, we get

$$\begin{aligned} M &= \left(1 - \left(\sinh\left(2\beta_I J\right)\right)^{-4}\right)^{\frac{1}{8}} \\ &= \left(1 - \left(\sinh\left(\frac{2J/T_c}{1+t}\right)\right)^{-4}\right)^{\frac{1}{8}} \\ &\approx \left(1 - \left(\sinh\left(\frac{2J}{T_c}(1-t)\right)\right)^{-4}\right)^{\frac{1}{8}} \end{aligned} \tag{3.18}$$

Deploying the addition theorems for sinh, we get

$$\begin{aligned} M &\approx \left(1 - \left(\underbrace{\sinh\frac{2J}{T_c}}_{=1}\cosh\left(\frac{2J}{T_c}t\right) - \underbrace{\cosh\frac{2J}{T_c}}_{=\sqrt{2}}\sinh\left(\frac{2J}{T_c}t\right)\right)^{-4}\right)^{\frac{1}{8}} \\ &= \left(1 - \left(\cosh\left(\frac{2J}{T_c}t\right) - \sqrt{2}\sinh\left(\frac{2J}{T_c}t\right)\right)^{-4}\right)^{\frac{1}{8}} \end{aligned} \tag{3.19}$$

Expanding the inner term to linear order in t yields

$$M \approx \left(1 - \left(1 - \sqrt{2}\frac{2J}{T_c}t\right)^{-4}\right)^{\frac{1}{8}}$$

After a final Taylor expansion we get

$$\begin{aligned} M &\approx \left(1 - \left(1 + \sqrt{2}\frac{8J}{T_c}t\right)\right)^{\frac{1}{8}} \\ &= \left(\sqrt{2}\frac{8J}{T_c}t\right)^{\frac{1}{8}} = \mathcal{O}\left(t^{\frac{1}{8}}\right). \end{aligned} \tag{3.20}$$

We can hence see that M is in leading order proportional to $t^{\frac{1}{8}}$. That means the theoretical critical exponent of M is $\beta = \frac{1}{8}$.

Similarly, the exponents ν of the correlation length and γ of the magnetic susceptibility can be derived to be 1 and $\frac{7}{4}$, respectively. The critical behavior of the specific heat is logarithmic, i.e. $\alpha = 0$.

Beyond the square-lattice model, there are no analytic solutions available in higher dimensions. However, simulations and renormalization group theory have been used to estimate critical exponents of the phase transition in the three-dimensional Ising model [39]. The exponents denoted in Table 1 are taken from [40].

3.3.2 Mean Field Theory

Mean field theories are a different class of physical models than what we described so far, however they are often (successfully) used to approximately describe behavior of Ising-like models. In the standard Ising model, spins only interact with their neighbors, while mean field Ising models instead consider each spin to be interacting with an average field induced by the other spins, i.e.

$$E = -\frac{qJ}{|V|-1} \sum_{(i,j)\in V\times V} \sigma_i \sigma_j. \tag{3.21}$$

where q is a normalization parameter. When considering the mean-field model to be derived from some "regular" Ising model, q can be considered to be the mean number of nearest-neighbors of the original model.

The mean-field Ising model can be solved analytically [37]. The study of critical behavior reveals the critical temperature

$$\beta_{c,I} = \frac{1}{qJ} \tag{3.22}$$

and the critical exponents $\beta = \frac{1}{2}$, $\alpha = 0$, and $\gamma = 1$. This means that the mean-field Ising model falls into a different universality class than the standard 2D model. However, for various other networks, mean-field theory matches the critical behavior of the standard Ising model. This includes lattices on dimensions higher than 4 and also many types of graphs with *far-range interactions*.

3.3.3 Cayley Trees and Bethe Lattices

Cayley trees are a certain class of finite, cycle-free graphs, for which the Ising model can be solved analytically. They are defined by starting from a central point 0 and adding q points (collectively called *first shell*) connected to the central point. From there, a new shell is constructed by adding $q-1$ vertices for each vertex in the first shell. The *second shell* then is constituted by the set of newly added points. The full tree is the result of repeated iteration of this procedure up to the n-th shell for some finite n. The *limit graph* obtained for $n \to \infty$ is called *Bethe lattice*.

The Ising model on both Cayley trees and Bethe lattices is solved analytically [37] using of the Bethe-Peierls approach [27, 28]. For Cayley trees, the free energy is an analytic function of the temperature, hence the standard second-order phase transition does not occur even in the thermodynamic limit. The lack of such a phase transition can be explained by "border" effects caused by the outermost shell [29]. While for other systems, one often finds that the fraction of border vertices within the total number of vertices converges towards zero with increasing system size, for Cayley trees both numbers grow exponentially in $q-1$.

On Bethe lattices, there are by definition no border vertices. Indeed, the analytic solution of the Ising model on such graphs exhibits the typical second-order phase transition

at the critical temperature

$$\beta_{BP} = \frac{\ln(q) - \ln(q-2)}{2kJ} \tag{3.23}$$

and assumes the critical exponents of the mean-field Ising model[12]. This is a remarkable result, since contrary to the mean-field model, Bethe-lattices are much closer to the regular square-lattice models since the interaction strength is independent from the network size and all interactions are "local" in the sense that only connected vertices interact with each other.

3.3.4 Scale-free uncorrelated Networks

A common property of random networks is the *degree distribution* $P(q)$ which denotes the probability for a randomly chosen vertex to be connected to q neighbors. A particular class of graphs is characterized by a degree distribution which is a power law with respect to some exponent τ, i.e.

$$P(q) \propto q^{-\tau}. \tag{3.24}$$

The critical behavior of the Ising model on scale-free networks is fully characterized for *uncorrelated* graphs, i.e. those which do not have any correlations between connected nodes.

The Ising model on such networks is approximately described using the exact recursion method [41] or using the replica trick [42]. Both methods come to the conclusion that the second-order phase transition is reproduced for $\tau > 4$, while values smaller than that exhibit higher-order phase transitions (up to infinite order for $2 < \tau \leq 3$). The exact transition temperature is

$$\beta_c = \frac{\ln\left(\frac{z_2+z_1}{z_2-z_1}\right)}{2J}, \tag{3.25}$$

with $z_1 = \langle q \rangle$ the mean number of nearest-neighbors and $z_2 = \langle q^2 \rangle - \langle q \rangle$ the mean number of the second nearest neighbors of a vertex[13]. The critical exponents α, β, and γ are known for the three classes $\tau > 5$, $3 < \tau < 5$, and $2 < \tau < 3$. The results are summarized in Table 1, but it is worth a note that the $\tau > 5$ case yields exponents matching the mean-field theory while the other cases show distinct behavior. It has been shown that these results are indeed accurate [43].

[12] In fact, for $q \gg 1$ the critical temperature also converges against the mean-field model.
[13] In fact, this result holds for generic uncorrelated graphs.

4 Lattice Triangulations

The aim of this section is to analyze the properties of the Ising model defined on lattice triangulations as explained in Section 3. In particular, we are interested in understanding whether the location of the phase transition of the standard two-dimensional Ising model or even its critical exponents change when moving to triangulations.

First, we define the notions of triangulations on a point lattice and edge flips. Then we introduce a method based on Monte-Carlo techniques to create all possible lattice triangulations. We analyze a particular lattice triangulation (called "perfectly ordered" for reasons explained later on) in full detail as a reference point and to illustrate our methods. After that, we look at statistical ensembles of random triangulations and of canonical triangulation states with respect to an order measure. Both of these ensembles are analyzed as quenched disorder, i.e. the Ising model properties are analyzed for each triangulation separately and then averaged (as opposed to annealed disorder, where the triangulation would be modified while simulating the Ising model).

In our analysis, we find that the Ising model on the perfectly ordered triangulation (see Section 4.2.2) is very similarly to the standard 2D square lattice model and in particular shares the same universality class with the latter. In Section 4.2.3, we furthermore see that the critical behavior among random ensembles of lattice triangulations is non-uniform and as such we cannot give single estimates for the critical exponents. Our results suggest that the critical exponents are distributed in regions close to the critical exponents of the 2D square-lattice model, however. Finally, our analysis of the canonical triangulation ensemble in Section 4.2.4 suggests that the order of a triangulation is directly linked to the critical behavior: Highly ordered triangulations on average have a high inverse critical temperature ($\beta_{c,I} \approx 0.30$), while unordered triangulations take a lower one ($\beta_{c,I} \approx 0.24$). Between those two extrema we find a crossover behavior, within which the ensemble behavior is described by random triangulations.

4.1 Terminology

We now introduce the basic notions used throughout this chapter, starting with the definition and properties of lattice triangulations, which can be interpreted as graphs and as such are used as the underlying network of an Ising model later. We then introduce a mean to quantify the *order* of a given triangulation, which we use as an *energy functional* to define canonical ensemble of triangulations later on. Finally, we define diagonal-edge flips, which are elementary transformations between two triangulations and which can be used to generate all triangulations of a fixed point lattice.

4.1.1 Lattice Triangulations

We consider a (full and unimodular) lattice triangulation $\mathcal{T}$ as a tiling of the (planar) $M \times N$ lattice spanned by the discrete point set

$$V(\mathcal{T}) = \left\{ \binom{m}{n} \in \mathbb{N}_0^2 \middle| \, m < M, n < N \right\} \tag{4.1}$$

using triangles (represented as the convex hull of three points in $V(\mathcal{T})$) such that the following conditions are met:

- Intersection-free: The interiors of two distinct triangles do not intersect
- Complete: two overlapping triangle borders either coincide or intersect in a vertex
- Full: Every point in $V(\mathcal{T})$ is the corner of at least one triangle
- Unimodular: All triangles have the same area (which is $\frac{1}{2}$ as a consequence of being full).

In the following, we will implicitly assume all lattice triangulations to be full and unimodular. Some examples of such triangulations are shown in Figure 3. It was shown by giving analytic bounds[44] and by performing explicit calculations[13] that the total number of such triangulations on a fixed lattice scales exponentially with the lattice size $M \times N$. This means that an extensive entropy can be defined on triangulations, which allows for applying standard tools of statistical physics.

One elementary property of any triangulation is the number of its edges. For the perfectly ordered state, this can be counted easily: Inner vertices are connected to six edges, border vertices to four, the bottom-left and top-right corner vertices to three, and the remaining corner vertices two edges. Summing over all vertices and dividing by 2 (the number of vertices that each edge connects) yields a total number of edges of

$$E = 3MN - 2M - 2N + 1 \tag{4.2}$$

on an $M \times N$ lattice (for $M \geq 2$ and $N \geq 2$). In fact, Equation (4.2) holds for any lattice triangulation, since there exists a transformation between any two triangulations which preserves the number of edges (as pointed out below, see Section 4.1.3). By comparison to the rectangular lattice, for which it is easy to count $2MN - M - N$ edges, one sees that for large lattices the average number of next-neighbors (obtained by dividing the edge count by the vertex count MN) is $\frac{3}{2}$ times the value of the square lattice. With regards to the Ising model, we hence expect an effective increase in the coupling constant due to the large number of neighboring spin interactions.

4.1.2 Order Measure

In the course of this work, we analyze the relation between the *order* of a triangulation and the critical phenomena of the Ising model on that triangulation. To this end, we introduce an energy functional describing the deviation from a previously chosen *ground state* $\mathcal{T}_0$. In accordance to prior work on triangulations [12] we choose

$$E_T(\mathcal{T}) := \sum_{v \in V(\mathcal{T})} \left(k_v^{(\mathcal{T})} - k_v^{(\mathcal{T}_0)} \right)^2, \tag{4.3}$$

with $k_v^{(\mathcal{T})}$ the number of edges incident with the vertex v within the triangulation $\mathcal{T}$. In other words, we define the energy as the sum of the squared deviation from the ground

state with regards to vertex degrees. Our choice of the ground state is depicted in Figure 3a. It is chosen such that it matches the authors' intuition of the *most ordered state* and hence will also be referred to as *perfectly ordered state*. This choice justifies calling $E_T(\mathcal{T})$ an order measure, since it describes the deviation from the most ordered state[14]. Our particular choice of the ground state could also be considered the least modification to the standard Ising model lattice, though. Note that the chosen state is non-degenerate with respect to the energy functional, since any modification will yield a non-zero term in Equation (4.3).

In Section 4.2.4, we look at averages of physical quanta within canonical ensembles of triangulations with respect to the energy defined in Equation (4.3). We denote the inverse temperature of this ensemble as α. Since triangulations are weighted with the Boltzmann factor $\exp(-\alpha E_T)$, the value $\alpha = 0$ corresponds to random triangulations while $\alpha = \infty$ suppresses any triangulations other than the perfectly ordered state (for which $E_T(\mathcal{T}_0) = 0$). We can also consider negative temperatures like $\alpha = -\infty$, for which the largest-energy triangulation dominates. The parameter α hence characterizes the *typical* order characteristics of triangulations in the ensemble. Typical states for each regime of α are shown in Figures 3a to 3c.

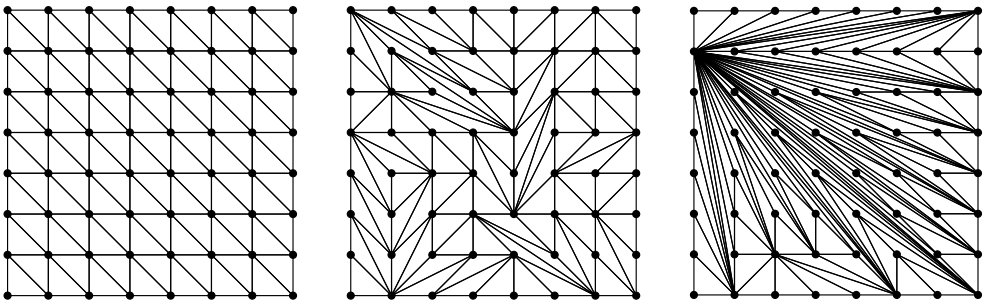

(a) $\alpha \to +\infty$ (b) $\alpha = 0$ (c) $\alpha \to -\infty$

Figure 3: Examples of unimodular 8×8 lattice triangulations. Figure 3a depicts the chosen perfectly ordered state with triangulation energy 0. Figure 3b is a randomly chosen triangulation. Figure 3c is one of the states with maximal triangulation energy. The comparison between the three examples shows how the defined energy functional $E_T(\mathcal{T})$ relates to disorder. The chosen examples may also be considered to be typical realizations of a canonical triangulation ensemble characterized by the parameter α, which for negative values introduces high-valent vertices and for positive values approaches the perfectly ordered state. The images are adapted from [12].

[14] As such, $E_T(\mathcal{T})$ actually measures the *disorder* of a triangulation, but we will use the term "order measure" regardless by abuse of notation.

4.1.3 Diagonal-Edge Flips

We are interested in the properties of ensembles of triangulations, rather than special properties of individual triangulations. For this purpose, we need a way to generate all triangulations on a given lattice. This can be achieved using so-called *diagonal-edge flips* (a certain kind of so called Pachner moves [45]), which are elementary transformations between two triangulations. The combination of multiple diagonal-edge flips allows for transforming a given triangulation into any other on the same lattice.

A diagonal-edge flip is initiated by selecting an edge $\{x_i, x_j\}$ of the triangulation at which two neighboring triangles $\{x_i, x_j, x_k\}$ and $\{x_i, x_j, x_l\}$ meet. Then, the quadrangle formed by these two triangles is considered: If it is convex, the two triangles are replaced by $\{x_i, x_k, x_l\}$ and $\{x_j, x_k, x_l\}$ (which corresponds to a "flip" of the quadrangle diagonal). If the quadrangle is concave, the flip is considered invalid and is discarded [46].

Obviously, diagonal-edge flips preserve the properties of the triangulations we consider — they transform full triangulations into full triangulations and unimodular ones into unimodular ones, and they do not change the number of edges in the graph. As such, they are well-suited for the construction of Markov chains. Furthermore, it was shown [47] that diagonal-edge flips are ergodic for triangulations of point sets in $\mathbb{R}^2$, hence enabling the application of Markov chain Monte Carlo methods. An example of a Markov chain constructed via diagonal-edge flips is displayed in Figure 4.

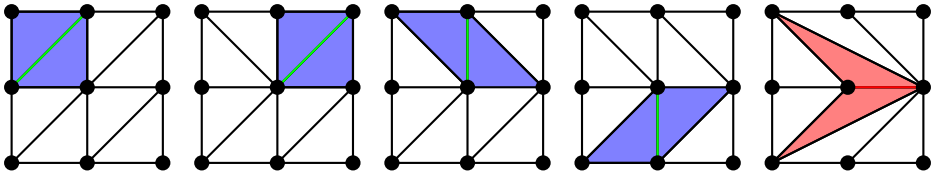

Figure 4: Example triangulation Markov chain obtained using diagonal-edge flips: The highlighted edge is randomly selected after each step and the quadrangle formed by the triangles meeting at that edge is considered. If the quadrangle is convex, the selected edge is flipped (first four chain elements). If it is concave, the flip is considered invalid (last element). Illustration by Benedikt Krüger.

The ergodicity of diagonal-edge flips allows for using them to model a state transition process of a Markov chain of $M \times N$ lattice triangulations with a probability distribution $P(\mathcal{T})$, following the algorithm outlined in Section 2.2.3. In particular, a random edge $e \in E$ of the current triangulation $\mathcal{T}$ is selected with probability $P_S(e) = 1/|E|$. We then generate a new triangulation $\mathcal{T}'$ by applying a flip around the selected edge. We then roll a number to decide whether or not to accept the new triangulation based on an acceptance probability $P_A(\mathcal{T} \to \mathcal{T}')$. This algorithm is started with the perfectly ordered triangulation and repeated until a sufficiently large number of triangulations has been generated.

In the context of the algorithm described in Section 2.2.3, using diagonal-edge flips as the state transition procedure determines[15] the selection probability $P_S(\mathcal{T}, \mathcal{T}')$, which

[15] In particular, the selection probability is zero for triangulations which are not connected by a valid

together with the acceptance probability $P_A(\mathcal{T} \to \mathcal{T}')$ determines the distribution $P(\mathcal{T})$ of triangulations occurring within the Markov chain. Hence, we must chose the acceptance probability P_A such that the algorithm yields the desired limit distribution $P(\mathcal{T})$. At the same time, the choice must guarantee that the detailed balance condition (2.17) is fulfilled. For random triangulation ensembles ($P(\mathcal{T}) = \text{const}$), this means we accept all selected diagonal-edge flips ($P_A(\mathcal{T} \to \mathcal{T}') = 1$), while for canonical triangulation ensembles ($P(\mathcal{T}) \propto \exp(-\alpha E_T(\mathcal{T}))$) we can express the acceptance probability in terms of the density of states $g(E_T)$ with respect to the energy functional $E_T(\mathcal{T})$ as $P_A(E \to E') = g(E)/g(E')$.

4.2 Critical Phenomena in the Ising Model

In this section, we present the results of our analysis of the Ising model on lattice triangulations. To this end, we first show a way to choose appropriate parameters of the Wang-Landau algorithm used for the simulations later on. Based on information obtained through the density of states in the Ising model, we then apply the methods outlined in Section 3.2 to determine the phase transition temperature and critical exponents for the perfectly ordered triangulation. Consecutively, we analyze the same properties on a quenched random ensemble of triangulations and finally consider a canonical triangulation ensemble based on the order measure (4.3).

4.2.1 Choice of Parameters for the Wang-Landau Algorithm

The quality of the results obtained by the Wang-Landau algorithm explained in Section 2.3 is crucial for quantitative results, since we use the density of states via flat histogram sampling for all subsequent computation of the system's observables. We hence now justify the choices of parameters and other implementation details used for the algorithm when determining the density of states of the Ising model[16] of a fixed triangulation.

Figure 5 shows the density of Ising states on the square lattice and on the perfectly ordered triangulation obtained using a sample run of the Wang-Landau algorithm for different boundary conditions. It can be seen that the DOS on the triangular lattice has a shape similar to the square-lattice but is skewed towards negative energies while preserving the maximum to be at the $E = 0$ state. Furthermore, using open boundary conditions rather than periodic ones narrows the diagram slightly. It should also be noted that the triangulation with open boundaries has very large entropy differences in the uppermost energy levels, which dramatically increases the time needed to obtain a flat histogram. This property is the reason we introduced a flexible energy cutoff in

diagonal-edge flip, and a constant value otherwise (since any edge of the triangulation is selected with equal probability).

[16] We also use another density of states obtained from the Wang-Landau algorithm for generating triangulations as explained in Section 4.1.3, where the energy functional is the order measure E_T of a triangulation. As noted in Section 4.2.4, this function was not computed in this thesis but reused from previous simulations performed within the research chair. This section hence entirely refers to the density of states with respect to the energy functional of the Ising model on a fixed graph.

Section 2.3.2 to ignore diagonal-edge flips leading to such energy levels[17] such that our simulations could be performed in a reasonable time frame.

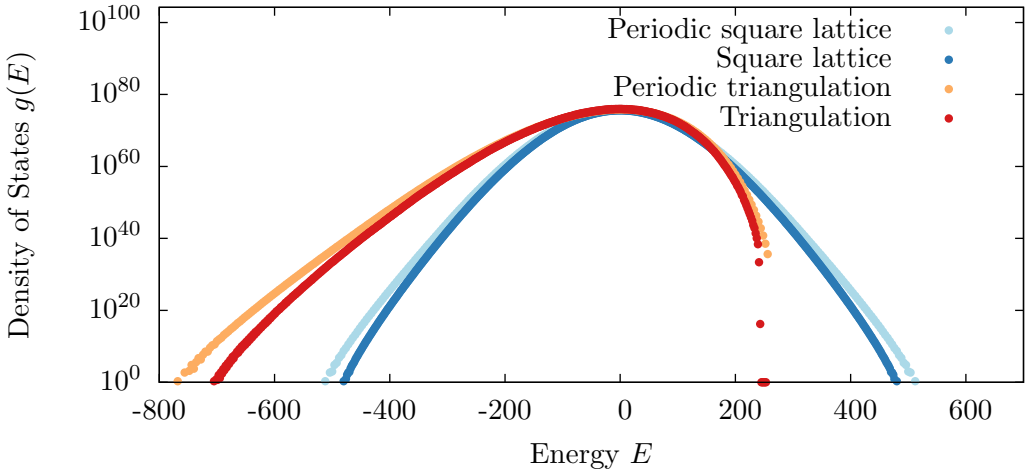

Figure 5: Comparison of the densities of state for various ordered systems on 16x16 lattices: While a square-lattice implies a symmetric DoS, the graph is skewed towards negative energies for lattice triangulations. The boundary conditions only play a secondary role. The DOS was computed using the Wang-Landau algorithm with the parameters $n = 0.9$, $f_{\text{final}} = 3 \times 10^{-7}$, and $p = 0.8$.

Other than this energy cutoff, we use conservative values for the Wang-Landau algorithm parameters $n = 0.9$ and $p = 0.8$ based on preliminary simulations which showed that higher values (which would yield more accurate simulation results) incur a significant increase in runtime. In the following we explicitly optimize for the final modification factor f_{final}, which marks the end of the simulation[18]. The need for a trade-off between accuracy and simulation time for this parameter becomes evident by looking at the number of total algorithm iterations it takes to progress to a particular modification factor f (cf. Figure 6). We see that the number of attempted diagonal-edge flips grows with a power of the logarithmic modification factor $\log f$.

To find a good value of f_{final}, we calculate the density of states ten times using different seeds for the random number generator. For each of the resulting DOSs we compute some scalar observable, and then consider the relative standard deviation of the ten resulting values. In Figure 7, we show this for the current density of state after each change to the modification factor f. The considered observable is $\langle E^2 \rangle = \sum E^2 g(E)$, but we could have used any other observable[19].The standard deviation will saturate for

[17] While arguably this is a modification to the model, the effect of the energy cutoff is negligible for ferromagnetic Ising models, in which the highest-energy states contribute the least to the partition sum.

[18] In particular, the simulation is stopped when the modification factor f takes a value *below* f_{final}.

[19] A restriction is that the observable should have a non-zero expectation value to be able to have a well-defined *relative* standard deviation. In particular this rules out $\langle E \rangle$, which is zero for the square lattice, as can be seen by the symmetric density of states (cf. Figure 5).

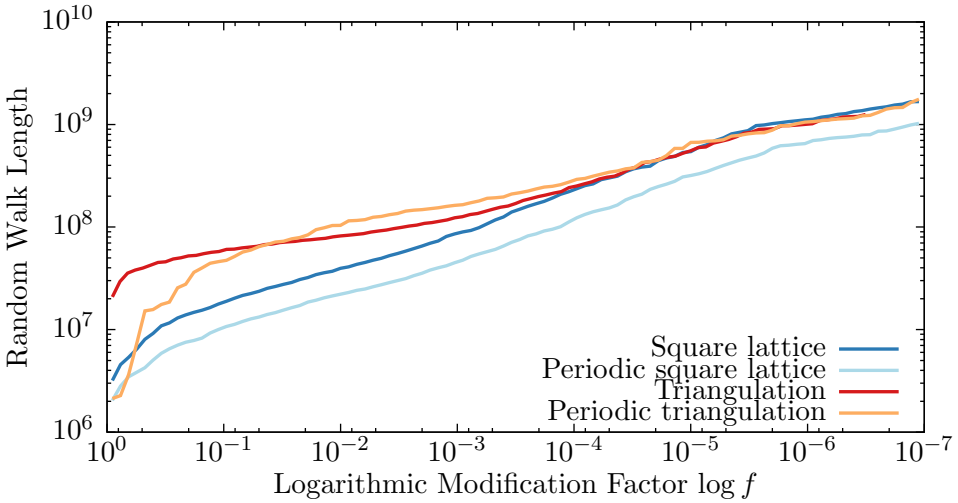

Figure 6: Comparison of the number of iterations required to progress while calculating the densities of state for various ordered systems on 16x16 lattices: While square lattices and periodic triangulations take roughly the same time to complete, free lattice triangulations require a lot more time.

large enough modification factor, so our choice of threshold should be "close enough" to the saturated regime.

To find a compromise between simulation time and quality of simulation results, we now consider the product of the absolute standard deviation of $\langle E^2 \rangle$ within ten runs and the number of random walk steps taken in the algorithm. Since $\langle E^2 \rangle$ is expected to decrease as the simulation progresses, the minimum of this product with respect to the current modification factor f (which can be considered a measure of simulation progress) loosely speaking denotes the point beyond which improvements to accuracy of results require a large amount of additional simulation runtime. We hence call this product "simulation cost" and plot it in Figure 8. The minimum can be found in the range $f \in [10 \times 10^{-6}, 10 \times 10^{-5}]$, with a moderate increase for smaller values of f. Including Figure 7 into considerations, we conclude that the choice $f_{\text{final}} = 1 \times 10^{-7}$ yields results which are accurate enough for our purpose and still can be computed within a reasonable amount of time.

4.2.2 Ground State Results

We now focus our attention on the properties of the Ising model on the ground state triangulation as defined in Section 4.1.2. The basis of all presented results is the density of Ising states obtained through the Wang-Landau algorithm, since we can use it to estimate any other system observable through flat histogram sampling (cf. Section 2.2.4). We first consider the specific heat (3.3) and the magnetic susceptibility (3.5) to verify on a basic level that the second-order phase transition is present on the triangular lattice, too. We then employ the Binder cumulant technique introduced in Section 3.2.2 to

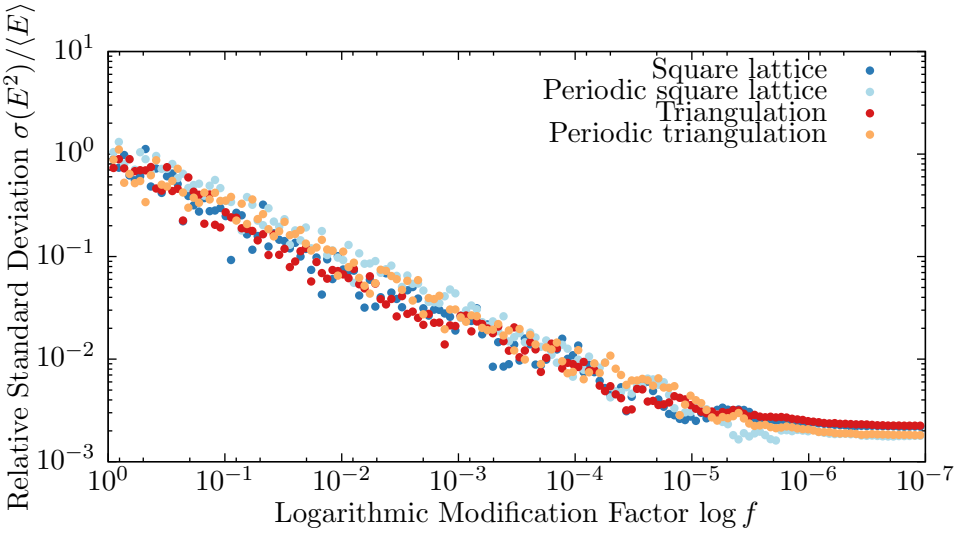

Figure 7: Dependence of the relative standard deviation of the average energy square $\langle E^2 \rangle$ over 10 Wang-Landau runs on the modification factor f of the algorithm. A power-law decay is observed until a modification factor of roughly 10^-5, beyond which it becomes increasingly hard to reduce the error any further. Simulations were performed on 8x8 lattices.

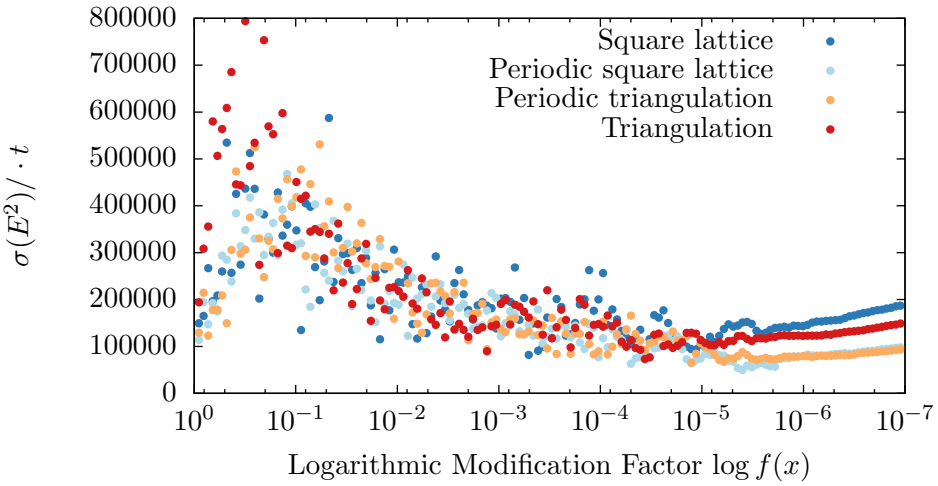

Figure 8: Change of "simulation cost" with the modification factor f of the Wang-Landau algorithm. We consider modification factors in the vicinity of the minimum in this plot to be good points of stopping the simulation.

analyze the properties at the critical point. We proceed with similar approaches when analyzing ensembles of lattice triangulations, hence this section also serves to illustrate the used methods in detail.

A characteristic property of the second-order phase transition in the Ising model is the singularity of the specific heat and the magnetic susceptibility at the critical temperature. In Figure 9, we plot these two observables for both the square lattice and the triangulation ground state. We see that in both plots there is no qualitative difference between the triangulation and the square lattice: Both observables fall off to zero for $\beta \to 0$ and $\beta \to \infty$ and assume a maximum which becomes more narrowly peaked as the system size increases, indicating a second order phase transition. The maximum, however, is shifted towards lower inverse temperatures β_I, which suggests that the critical temperature in this model has a different value. As we explain later, this is due an effective increase in the coupling constant J.

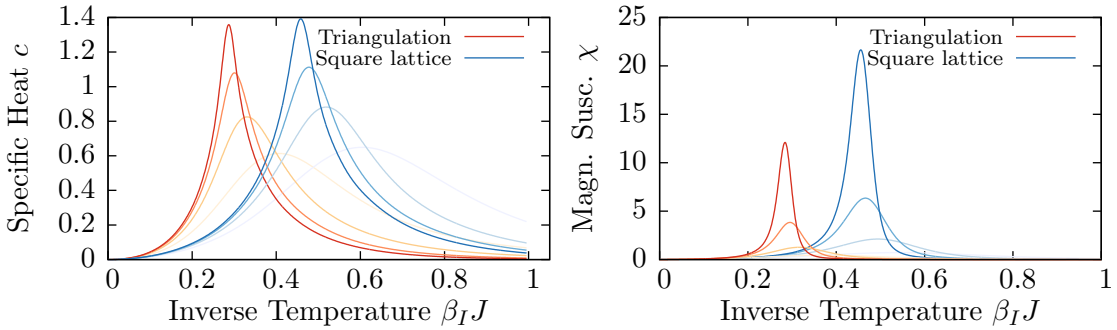

Figure 9: Plot of two the specific heat and magnetic susceptibility of the canonical ensemble in the Ising model, both for the square lattice (blue) and the triangular lattice (red). Each graph corresponds to a particular lattice size (with increasing color intensity: 4x4, 8x8, 16x16, 32x32)

To quantitatively determine the critical temperature, we use the Binder cumulant method described in Section 3.2.2, which involves determining the intersection points of $U_L(\beta_I)$ curves for different lattice sizes. We can locate the intersection of two such curves with quasi-infinite resolution in β_I, since flat histogram sampling is independent from the system temperature and evaluating canonical expectation values after sampling is computationally cheap as explained in Section 2.2.4. This means the intersection points can be determined using binary search with regards to β_I. The $U_L(\beta_I)$ curves are shown in Figure 10. The resulting intersection points are listed in Table 2. As expected, the Binder cumulants indeed intersect approximately in the same point regardless of the system size. Due to the comparatively small lattice sizes, we estimate the critical temperature to be equal to the value obtained from the intersection point of the $L = 8$ and $L = 16$ curves. We denote the uncertainty of this estimate as the difference to the intersection point of the $L = 4$ and $L = 8$ curves. This yields $\beta_{c,I} = 0.275 \pm 0.003$ for the periodic triangulation lattice. This method manages to reproduce the analytic solutions for the periodic square ($\beta_{c,I} \approx 0.44069$ as implied by Equation (3.16)) and triangular

($\beta_{c,I} \approx 0.27465$ according to [37]) lattices well. This change can partially be explained by considering that the number of edges incident per vertex is increased by the factor $\frac{3}{2}$ (cf. Section 4.1.1) when comparing the triangulation to the square lattice. This can be interpreted as an effective increase of the coupling constant and as per Equation (3.16) hence an effective decrease of the inverse critical temperature by the same factor. This idea yields $\beta_{c,I,\text{expected}} \approx 0.29379$, which is close enough to the true value to conclude that this effect indeed explains why the inverse critical temperature is smaller on the triangular lattice. Throughout this analysis, the boundary conditions had no relevant impact on the results.

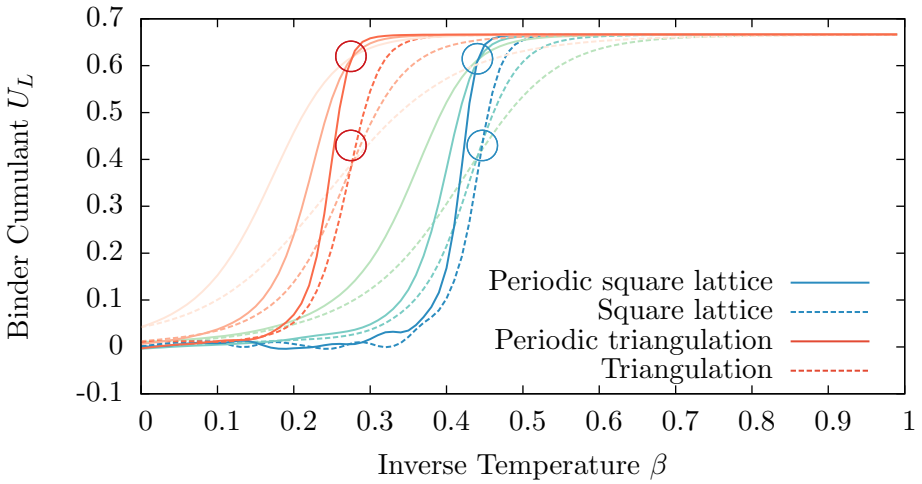

Figure 10: Binder cumulants for different lattice types and boundary conditions: For each lattice type, the curves meet almost perfectly in a single point regardless of the system size. The intersection points are used as estimates for the critical temperature. Considered system sizes are L=2,4,8.

Table 2: Intersection points of Binder cumulant functions $U_L(\beta_I)$ across different system sizes L_1 and L_2. We take the intersection point for $L_1 = 8$ and $L_2 = 16$ to estimate the critical temperature of the system.

		Square Lattice		Triangular Lattice	
L_1	L_2	open	periodic	open	periodic
2	4	0.5269	0.2757	0.2782	0.1764
4	8	0.4585	0.4502	0.2747	0.2777
8	16	0.4406	0.4421	0.2742	0.2750

The next step in our analysis is to determine the values of critical exponents, starting with ν. As explained in Section 3.2.2, the slope of the Binder cumulant is expected to be proportional to $L^{1/\nu}$ (cf. Equation (3.12)). This allows extraction of the critical exponent ν using a linear fit in the double-logarithmic plot, which we show in Figure 11. The values we obtain are summarized in Table 3.

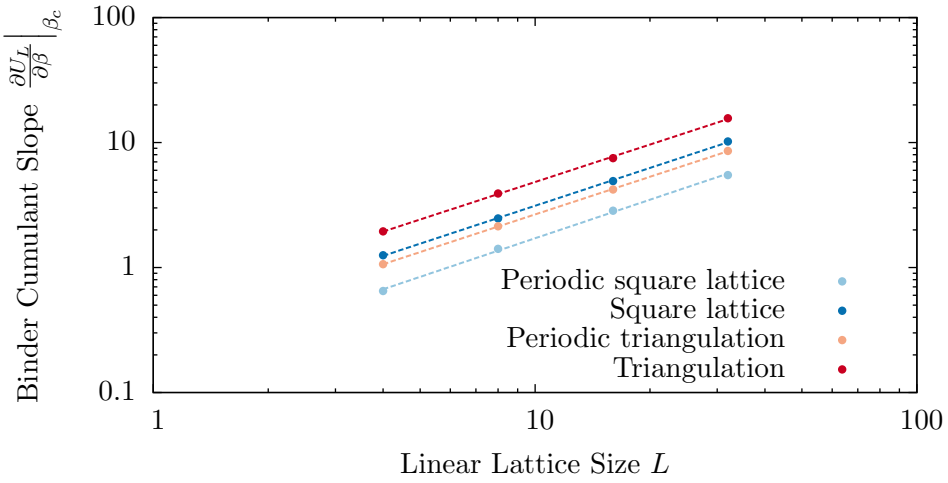

Figure 11: Exponential fit to the slope of the Binder cumulant as a function of the linear system size L. The obtained exponent provides an estimate for the inverse critical exponent $1/\nu$.

Table 3: Critical temperature and exponent ν derived from Binder cumulant comparison for different lattice types. The denoted errors are fit errors of the Marquardt-Levenberg algorithm as reported by gnuplot.

lattice type	β_c	ν	$-\beta/\nu$	γ/ν
square	0.441	1.006 ± 0.014	-0.218 ± 0.010	1.621 ± 0.024
periodic square	0.442	1.025 ± 0.028	-0.112 ± 0.003	1.745 ± 0.028
triangulation	0.274	1.000 ± 0.016	-0.193 ± 0.013	1.618 ± 0.029
periodic triangulation	0.275	1.001 ± 0.006	-0.119 ± 0.001	1.761 ± 0.005

To obtain the other critical exponents, we use the finite-size scaling ansätze

$$m \propto L^{-\beta/\nu} \tag{4.4}$$

and

$$\chi \propto L^{\gamma/\nu} \tag{4.5}$$

as introduced in Section 3.2.1. Since these relations are expected to hold even at temperatures which are slightly off the true critical temperature (so in particular for our estimate of $\beta_{c,I}$), we can estimate the values of $\frac{\beta}{\nu}$ and $\frac{\gamma}{\nu}$ using a fit to these equations. The double-logarithmic plots in Figure 12a and Figure 12b show that this is working well regardless of lattice type and boundaries. Our quantitative results are listed in Table 3.

Looking at the critical exponents in Table 3, we see excellent agreement of the critical exponent ν, which was extracted from the Binder cumulant, in the perfectly ordered triangulation with the value of the standard 2D Ising model. For the other exponents, boundary conditions make a huge difference, since the finite-size effects have a larger impact on the observables χ and m than on the Binder cumulant. While the estimated

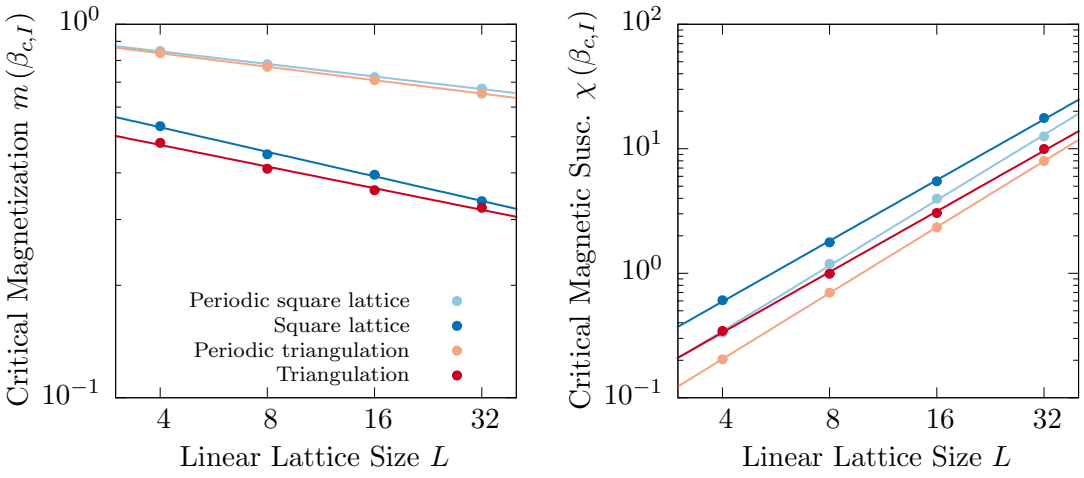

(a) β (b) γ

Figure 12: Exponential fits to the values of m and χ at the critical point as functions of the linear system size L. The resulting exponents provide estimates for the ratios of critical exponents $\frac{\beta}{\nu}$ and $\frac{\gamma}{\nu}$.

values for lattices with open boundaries are somewhat off from the analytically known one in the standard 2D Ising model, our observed behavior of the triangular and the square lattice models match. Our conclusion is that the critical exponents do not change when moving to the Ising model on the perfectly ordered triangulation. In other words, changing the Ising model to use a triangular lattice does not change its universality class.

4.2.3 Random Triangulation Ensemble

We now consider an ensemble of random triangulations, generated according to the procedure outlined in Section 4.1.3 and distributed uniformly by choosing the flip acceptance probability $P_A(\mathcal{T}_i \to \mathcal{T}_j) = 1$. To analyze the phase transitions, we use the same techniques as for the perfectly ordered triangulation discussed in Section 4.2.2, although some modifications are applied for analysis of an ensemble (as opposed to a single triangulation).

First, we look at the generic system behavior by plotting the specific heat for 100 ensemble realizations. Figure 13 shows the resulting C-β_I-diagram for different lattice sizes. It can be seen that different triangulations yield different runs of the curve, but overall the qualitative behavior is shared among the ensemble and hence making the specific heat appear as a smeared version of the ground state curve. The fact that curve maxima are also varying suggests that the critical temperature distribution is smeared similarly. It is interesting to note that the perfectly ordered triangulation shows a very non-standard behavior, suggesting that the disorder introduced in the random ensemble does have a noticeable effect on the behavior of the Ising model.

To analyze the distribution of the critical Ising temperature $\beta_{c,I}$, we again compare the

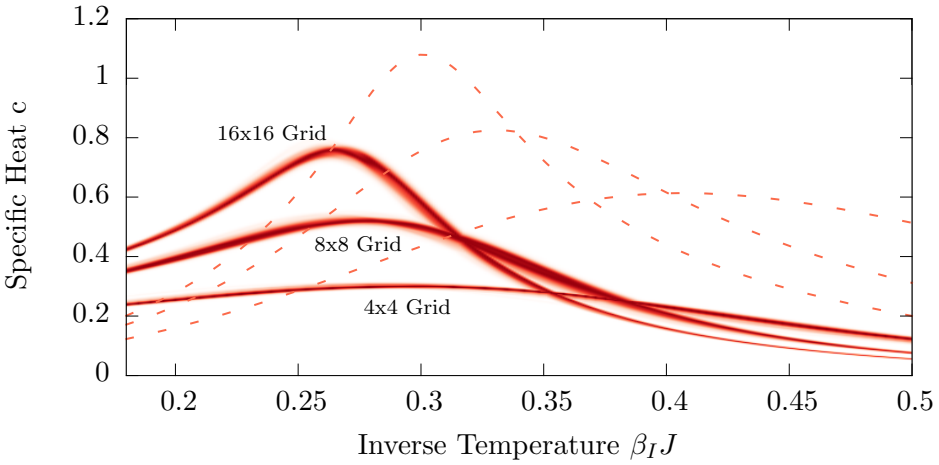

Figure 13: Specific heat c of a random ensemble of lattice triangulations. The color intensity of each pixel in the picture is proportional to the number of $c(\beta_I J)$ curves that cover the pixel. The perfectly ordered triangulation for each of the considered lattice sizes is plotted in dashed lines.

Binder cumulant between different system sizes. In particular, for each $L \times L$ ensemble triangulation, we locate the Binder cumulant intersection point with each of the $2L \times 2L$ ensemble triangulations. The distribution obtained by performing this for 100 triangulations of each lattice size are shown in Figure 14. We find that this distribution takes the shape of an increasingly narrow normal distribution as the lattice size increases. For the comparison between the 16x16 and 32x32 triangulations, we find a mean value of 0.246482 and a standard deviation of 0.006.

The fact that there is no single, well-defined value of the critical temperature is a problem for determining critical exponents, which by our method require evaluation of the Binder cumulant slope and other observables at some fixed critical temperature. Ideally, one would hence only include subsets of triangulations with similar quasi-critical temperature for the evaluation of these slopes. For simplicity, we went for a different approach: For each lattice size (the number of which we refer to as N_L) we pick one triangulation out of the ensemble, such that we obtain an N_L-tuple of triangulations. The idea is then to compute both a critical temperature and the critical exponents, so that errors stemming from using the "wrong" critical temperature are reduced. The critical temperature is determined as before from the Binder cumulant intersection points, based upon which the inverse critical exponent $1/\nu$ is calculated by fitting a power law with respect to the system size against $\left.\frac{\partial U_L}{\partial \beta_I}\right|_{\beta_{c,I}}$. Similarly, we estimate $-\beta/\nu$ and γ/ν by fitting a power law with respect to the system size against $m(\beta_{c,I})$ and $\chi(\beta_{c,I})$, respectively. We generate 5000 triangulation tuples on which these values are calculated and collect the results as a distribution shown in Figure 15.

The two fit exponents $-\beta/\nu$ and γ/ν roughly take the shape of a normal distribution,

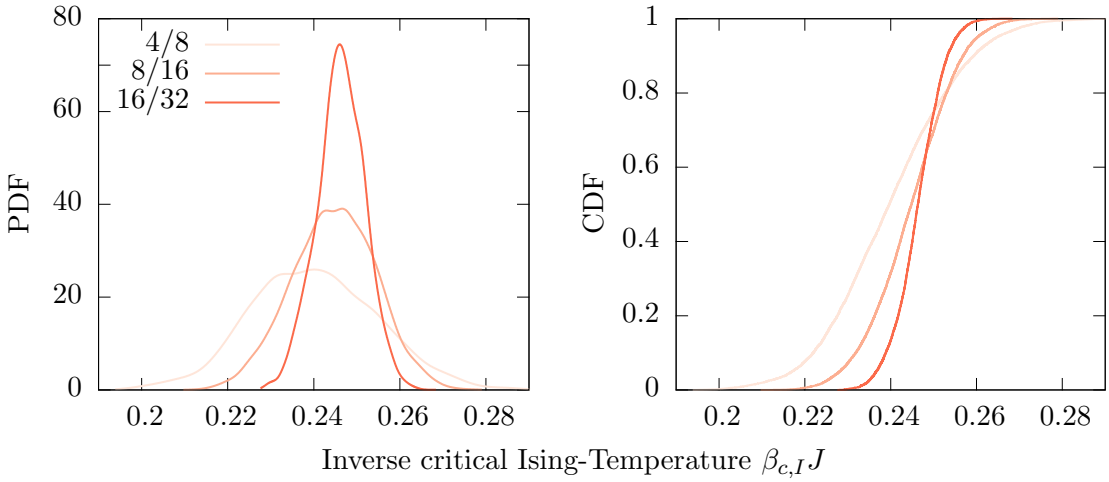

Figure 14: Probability density function (PDF) and cumulative distribution function (CDF) of the estimated critical inverse temperatures among random lattice triangulations. The results were obtained from the Binder cumulant intersection points of each one out of 100 small lattices ($L \times L$) compared against each one out of 100 large lattices ($2L \times 2L$) with L and $2L$ denoted in the legend. Increasing colors intensity corresponds to larger lattices.

and the fit error margins have a uniform error magnitude for all data points. Our method seems to work less well when looking at the distribution of the exponent $1/\nu$ though, which has a very broad probability density and strongly scattered error distribution. This requires some justification: The peak structure resembles that of a normal distribution, but outside of that the distribution broadens up significantly. The "off-peak" data points ($\nu < 0.5$) have a very large absolute fit error though and hence may be considered invalid, such that merely the peak structure will be considered valid.

As a cross check, we tried a different approach by first averaging the Binder cumulant pointwise for 100 realizations of each system size and by then estimating the critical exponent ν using the averaged Binder cumulants. From this we cannot draw any conclusion of the distribution of critical temperature or exponents, but it's an indicator for the typical values. As seen in Figure 16, there is no definite intersection point, but we can estimate the critical temperature to be between 0.24 and 0.25. The lack of precise estimation does not hinder us from performing a power-law fit, since the binder cumulant derivative changes slowly within the vicinity of the critical temperature. We hence perform these fits at different points and see that the inverse critical exponent ν obtained lies in the range 0.88–0.93. This is consistent with the prior results, which showed the distribution of the inverse critical exponent to be peaked in a similar range.

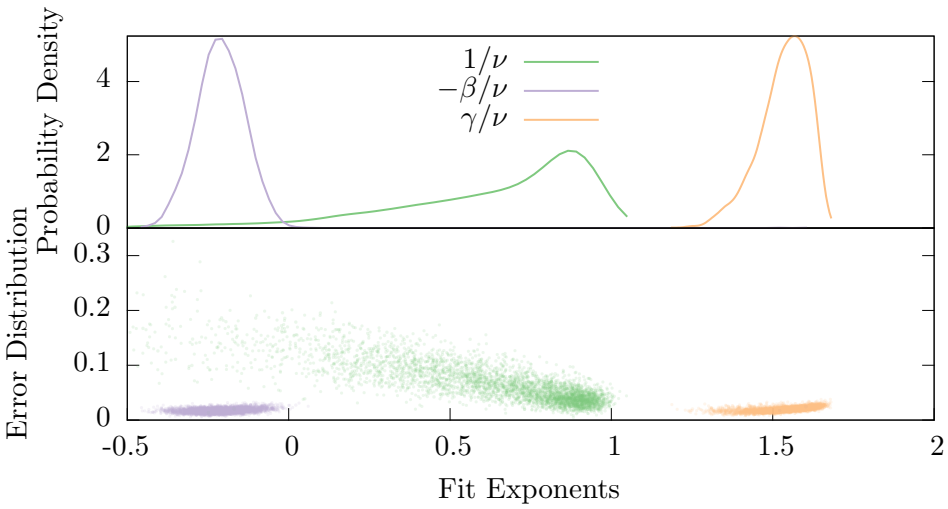

Figure 15: Distribution of fit exponents $1.0/\nu$, $-\beta/\nu$, and γ/ν among random lattice triangulations. The upper plot shows the kernel density estimation of the exponent distribution, while the bottom plot shows the magnitude of (absolute) fit errors for each reference tuple.

4.2.4 Canonical Triangulation Ensemble

As the next step, we want to understand how specifically triangulation order influences the critical exponents of the Ising model. For this purpose, we generate a canonical ensemble of triangulations with respect to the triangulation order functional, the realizations of which we construct using a Markov chain generated using diagonal-edge flips. Since the detailed balance condition should be fulfilled, the acceptance probability for diagonal-edge flips needs to be chosen appropriately as explained in Section 4.1.3. For this purpose, we need to know the density of states $g_T(E_T)$. We did not compute this as part of this thesis, but instead used prior results [13] which were obtained using the Wang-Landau algorithm. Since this approach is very computationally expensive, we are limited to very small lattice sizes ($L \leq 10$).

Within this canonical triangulation ensemble, the Ising model is implemented as a system of quenched disorder, i.e. quantities like the Ising model's critical temperature and exponents themselves are evaluted for each triangulation separately and the results are then averaged over the ensemble of triangulations. In particular, this is implemented by entropically sampling a number of triangulations and computing a quantity of interest (denoted as I for the purpose of this description) for each of them. For each triangulation energy level, the microcanonical averages $\langle I \rangle_{\text{mc}}(E_T)$ are computed. The final canonical ensemble average of I then is

$$\langle I \rangle_{\text{can}}(\alpha) = \frac{\sum_{E_T} \langle I \rangle_{\text{mc}}(E_T) g_T(E_T) e^{-\alpha E_T}}{\sum_{E_T} g_T(E_T) e^{-\alpha E_T}}. \tag{4.6}$$

In the context of critical phenomena, the small lattice size implies that we cannot apply any of the Binder cumulant methods used before: As seen in the regime of small

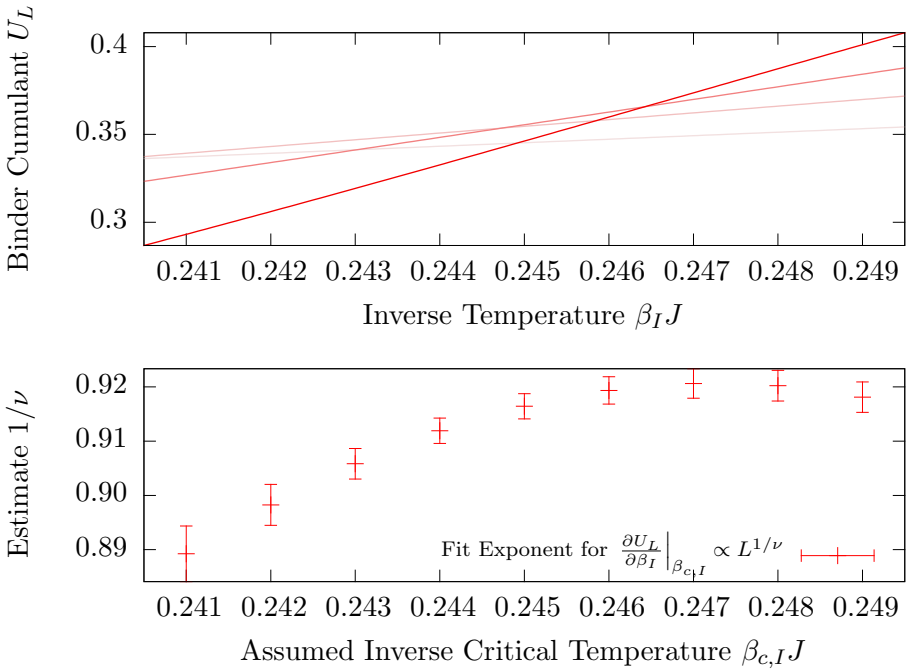

Figure 16: Determining critical exponents based on averaged Binder cumulants: The top plot shows the run of the Binder cumulant averaged over 100 realizations for each system size (4x4, 8x8, 16x16, 32x32). The bottom plot provides estimates for the inverse critical exponent $1/\nu$ by evaluating a power law fit at different values of β_I.

lattices in Table 2, estimates for the critical temperature obtained via Binder cumulant intersections may be relatively strongly affected by finite-size effects. Furthermore, we previously compared only $L \times L$ and $2L \times 2L$ lattices against each other, but since we are capped at $L = 10$, we need to include comparisons of lattices with smaller size differences in order to have more than two data points. Since the Binder cumulants of such lattices will differ much more subtlely, our estimates would become very inaccurate.

Instead, we estimate the critical Ising temperature for each realization by determining the maximum of the magnetic susceptibility. Figure 17 shows the canonical expectation values for varying α and different lattice sizes. We observe a crossover behavior with regards to the order measure at $\alpha \to 0$. For large lattices, the critical Ising temperature of disordered triangulations is approximately 0.24, while for ordered triangulations we obtain a value of 0.30. Note that the latter value does not match our previous results in Section 4.2.2 where we analyzed the perfectly ordered triangulation on its own. This is because we were using the FSS ansätze in this section, while in Section 4.2.2 we were using Binder cumulant considerations, which are less prone to finite-size effects. This means that the value 0.24 also needs to be taken with a grain of salt, however.

To determine critical exponents, we tried the method of looking at individual N_L-tuples of triangulations as outlined in Section 4.2.3. However, the results were scattered

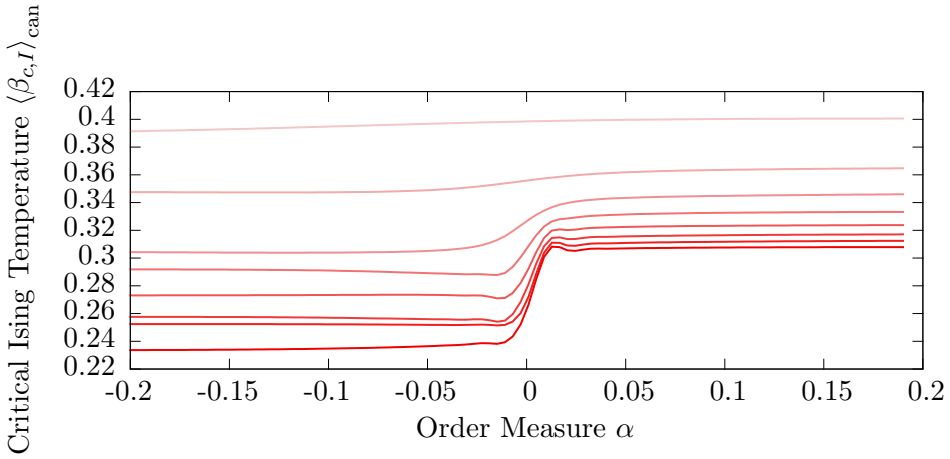

Figure 17: Change of critical Ising temperature with order of the triangulation ensemble: The curve color represents, with increasing intensity, the lattice sizes 3×3 through 10×10. For large lattices, there is a plateau at highly ordered triangulations and another one at highly disordered triangulations. Between the two regions, there is a crossover behavior at $\alpha = 0$, at which the random ensemble properties are attained.

much more broadly and the error estimates rendered the results useless. Focusing on the critical behavior of the magnetic susceptibility, we hence pursue an alternative attempt by computing an ensemble-average of the function $\chi(\beta_I)$. From this ensemble average, we obtain an estimate for the critical temperature $\beta_{c,I}$ by precisely locating the curve maximum using a ternary search. In zeroth order, this estimate should not deviate from computing the critical temperature for each realization and then averaging the result. We plot $\chi\left(\frac{\beta_{c,I}-\beta_I}{\beta_I}\right)$ for highly ordered systems ($\alpha = 10$) and try to obtain the critical exponent γ/ν via a power-law fit in the vicinity of the critical temperature. As seen in the top plot of Figure 18, no part of the curve appears to be a good candidate for linear fitting. Furthermore, even though the order measure $\alpha = 10$ should yield triangulations akin to the perfectly ordered triangulation discussed in Section 4.2.2, an $x^{-1.75}$ curve clearly is steeper than the plot data at any point. Indeed, repeating the same measurement with the actual perfectly ordered triangulation (cf. the bottom plot in Figure 18), we see that system sizes 4x4 and 8x8 yield results far off from the true critical exponents, and good results cannot be obtained below 32x32 grids.

Due to these observations, we conclude that for a proper discussion of critical exponents, access to greater system sizes is required (which is unlikely to be possible with the Wang-Landau algorithm due to impractical computational effort as lattice sizes grow) or finite-size corrections need to be considered.

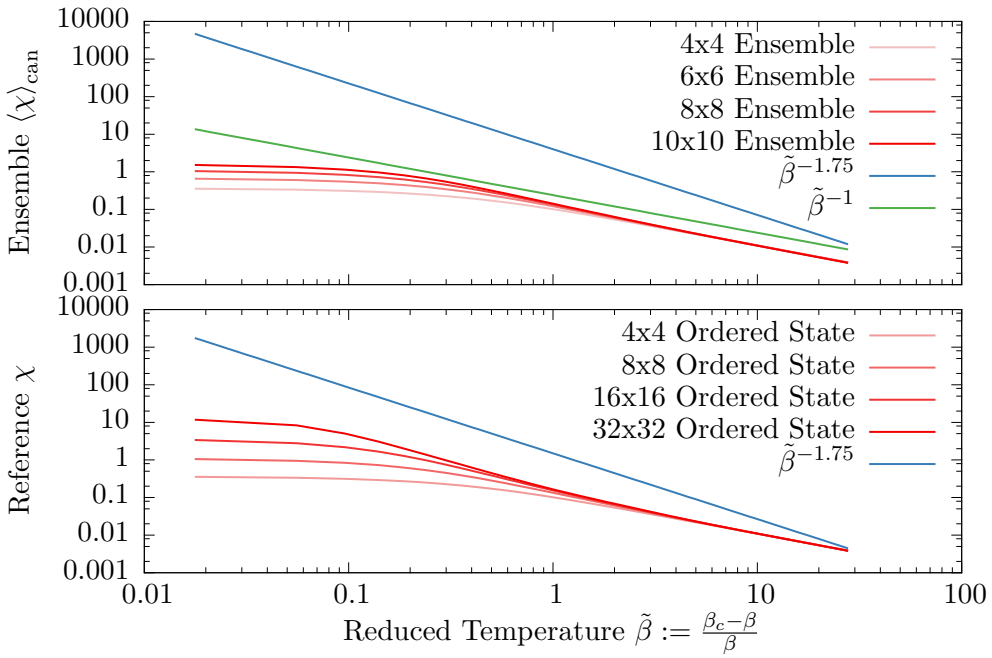

Figure 18: Top: Mean of the magnetic susceptibility (red curve) in the canonical triangulation ensemble at $\alpha = 10$ (corresponding to highly ordered triangulations) in the vicinity of the critical Ising temperature: While due to the results discussed in Section 4.2.2 we expect an $x^{-1.75}$ power-law fit to be possible somewhere in this regime, the curve doesn't show resemblance to a power law at any point. An x^{-1} fit comes close, but it's too far away from the critical point to be relevant for the discussion of critical exponents. For reference, the bottom plot shows the behavior of the perfectly ordered system at larger lattice sizes, where a $x^{-1.75}$ power-law can be seen for $\tilde{\beta} \in [0.1; 1.0]$.

5 Topological Triangulations

We now consider a different class of triangulations, which are not defined on a fixed, two-dimensional point set in Euclidian space, but instead on closed two-dimensional topological manifolds. In particular, this means we ignore the actual vertex coordinates of the triangulation and only consider topological degrees of freedom (i.e. the connection of vertices). In this chapter, we analyze the properties of such triangulations in terms of characteristic properties like total vertex number V and genus g (which equals the genus of the underlying manifold). We first introduce the required terminology and algorithms, and then analyze the properties of random ensembles of the Ising model phase transition on quenched random ensembles of topological triangulations.

In our analysis we find that the genus of a topological triangulation determines how the quasi-critical temperature $\beta_{c,I}$ changes with increasing system size (see Figure 22). We believe this behavior can be explained by considering an effective change in the coupling constant when the ratio of the number of edges to the number of vertices in the triangulation changes as described by Equation (5.10). Assuming the given explanation to be true, we extrapolate the value of the critical temperature in the thermodynamic limit and show in Figure 23 that with increasing genus, the critical temperature decreases.

5.1 Topological Triangulations and Flips

This chapter explains the mathematical concepts involved to define topological triangulations, and introduces a notion of flips similar to the diagonal-edge flips introduced in Section 4.1.3. The terminology and definitions mentioned here are following [48, 49].

5.1.1 Topological Triangulations

A topological triangulation represents topological and geometric properties of a manifold M in terms of triangles (or, more generally, their analoga in other dimensions called *simplices*). The topological information (i.e. connectivity relations between triangles and their edges) is captured in what's called an *abstract simplicial complex*, while geometric information is described in terms of an embedding of the abstract simplicial complex into an Euclidian space $\mathbb{R}^m$ with $m > d$.

To be able to generalize our results to any dimension, we first replace our use of the term "triangles" with the more generic notion of an n-simplex, which is the (closed) convex hull of $n+1$ linearly independent[20] points in $\mathbb{R}^m$. In particular, points, lines, triangles, and tetrahedra are 0-, 1-, 2-, and 3-simplices, respectively, and it's easy to see that this generalizes trivially to higher dimensions.

Building upon simplices, properties of polyhedra can be encoded using *simplicial complexes*. A simplicial complex $\mathcal{S}$ is a set of simplices in a fixed Euclidian space which is closed under intersection of simplices,

$$\sigma, \sigma' \in \mathcal{S} \Rightarrow \sigma \cap \sigma' \in \mathcal{S}, \tag{5.1}$$

[20] Linear independence of point sets in Euclidian spaces is defined in terms of linear independence of connecting vectors of one fixed reference vertex from the set to the remaining vertices.

and also closed under formation of subsimplices

$$\sigma \in \mathcal{S}, \sigma \subset \sigma' \Rightarrow \sigma' \in \mathcal{S}, \tag{5.2}$$

for any two simplices σ and σ'.

An *abstract simplicial complex* $\mathcal{K}$ generalizes simplicial complexes in that it does not refer to any particular Euclidian space: It is defined as a set of subsets of some index set $\mathcal{I}$ (i.e. it is a subset of the index set's power set, $\mathcal{K} \subset 2^{\mathcal{I}}$), such that

$$\sigma, \sigma' \in \mathcal{K} \Rightarrow \sigma \cap \sigma' \in \mathcal{K}. \tag{5.3}$$

and

$$\sigma \in \mathcal{K}, \sigma' \subset \sigma \Rightarrow \sigma' \in \mathcal{K} \tag{5.4}$$

From this definition it is apparent that any simplicial complex is trivially also an *abstract* simplicial complex by labeling each 0-simplex (i.e. corner vertex) with a unique number and then labeling any higher-dimensional simplex with the union of its subsimplices' labels. Even though an abstract simplicial complex $\mathcal{K}$ is solely defined in set theoretic terms, it can be shown that for any $\mathcal{K}$ there is an invertible map to a simplicial complex $|\mathcal{K}|$ [48]. The image of this map is furthermore unique up to homeomorphisms and hence we call $|\mathcal{K}|$ the *geometric realization of* $\mathcal{K}$. In this sense, Equations (5.3) and (5.4) are equivalent to (5.1) and (5.2).

Putting these notions together, we define a *(topological) triangulation* of a manifold M as a pair $(\mathcal{K}, h)$ of an abstract simplicial complex $\mathcal{K}$ and a homeomorphism h from a particular geometric realization $|\mathcal{K}|$ to M.For the purpose of illustration of triangulations, it's easiest to display the image of the homeomorphism h as a triangulated mesh. In Figure 19, we show example triangulations of the 2-sphere and the torus.

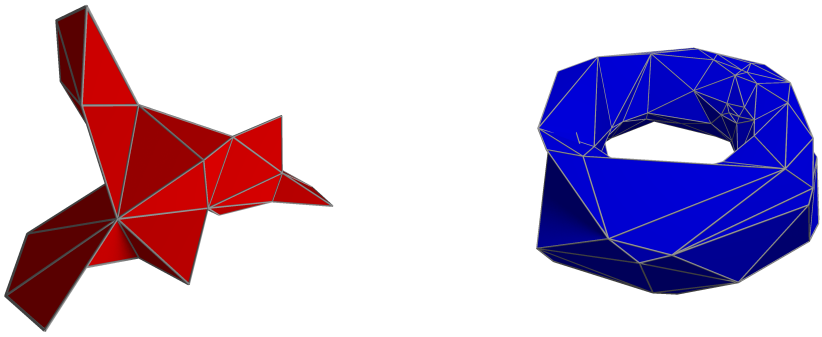

Figure 19: Examples of topological triangulations of the sphere ($g = 0$, left) and the torus ($g = 1$, right). Images taken from [50].

This thesis will only be concerned with topological surfaces, i.e. two-dimensional manifolds, which are classified by their Euler characteristic χ. The Euler characteristic is fully encoded in the abstract simplicial complex $\mathcal{K}$ of a triangulation of a manifold M, since for surfaces we have

$$\chi(\mathcal{K}) = V(\mathcal{K}) - E(\mathcal{K}) + T(\mathcal{K}) \tag{5.5}$$

where $V(\mathcal{K})$, $E(\mathcal{K})$, and $T(\mathcal{K})$ are the number of points (0-simplices), lines (1-simplices), and triangles (2-simplices) of $\mathcal{K}$, respectively. We will not work with the Euler characteristic directly, but instead use the *genus*, which can be computed from the Euler characteristic via

$$g(\mathcal{K}) = \begin{cases} \frac{1}{2}\left(2 - \chi(\mathcal{K})\right), M \text{ orientable} \\ 2 - \chi(\mathcal{K}), M \text{ non-orientable} \end{cases} \tag{5.6}$$

In the following, we will consider orientable surfaces, only, but our methods can easily be generalized to non-orientable surfaces, too.

5.1.2 Pachner Flips

To generate ensembles of topological triangulations, we employ transformations similar to the flips on lattice triangulations discussed in Section 4.1.3. However, the lack of geometry and fixed point coordinates adds some complexity, since we are no longer bound to a fixed number of vertices but may add or remove individual vertices. We use elementary operations called *Pachner flips* [45] to describe this. For triangulations of two-dimensional manifolds, Pachner flips are categorized into three classes, which are outlined in this section.

One such class are diagonal-edge flips, which work analogously to lattice triangulations by flipping the diagonal within a quadrangle. While there is no fixed geometry (and hence no restrictions with regards to convexity apply), care must be taken not to destroy the triangulation by the flip — which may happen when the selected would introduce a simplex into the triangulation which was already part of it[21]. Formally, a diagonal-edge flip is implemented by first picking two triangles $\sigma_1 = \{v_i, v_j, v_k\}$ and $\sigma_2 = \{v_i, v_j, v_l\}$, which share the common edge $\{v_i, v_j\}$. These two triangles (and correspondingly their subsimplices) are then replaced with $\sigma_1' = \{v_k, v_l, v_i\}$ and $\sigma_2' = \{v_k, v_l, v_j\}$. The process is illustrated in Figure 20a.

The other two kinds of Pachner flips are insertion and removal flips. Insertion flips insert a new vertex into a triangulation and thereby replace a single triangle by three new ones (cf. Figure 20b). Formally, the triangle $\sigma = \{v_i, v_j, v_k\}$ is replaced with the triangles $\sigma_1' = \{v_i, v_j, v_l\}$, $\sigma_2' = \{v_j, v_k, v_l\}$, and $\sigma_3' = \{v_k, v_i, v_l\}$, with v_l being the introduced vertex. For each insertion flip there is an inverse step defined in the obvious way by removing the vertex common to three adjacent triangles from the triangulation, hence replacing the triangles σ_1', σ_2', and σ_3' with σ.

We will use insertion/removal flips to *grow/shrink* topological triangulations to the desired system size in vertices: Insertion flips can be rolled by selecting a random triangle of the triangulation to subdivide, while removal flips are rolled by selecting a random vertex of the triangulation. Diagonal-edge flips will be used as a mean to *randomize* triangulations while keeping the system size constant, and are rolled as before by selecting a random edge.

[21] An example of such an invalid diagonal-edge flips can be seen in the tetrahedron triangulation, which any diagonal-edge flip would degenerate into two triangles.

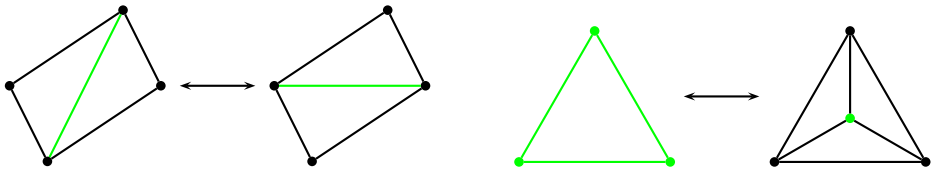

(a) Diagonal-edge (b) Insertion/Removal

Figure 20: Illustration of the three classes of Pachner flips in topological triangulations: Diagonal-edge flips (left) and insertion/removal flips (right). The colored object defines the flip and is randomly selected out of the full triangulation.

All of these operations preserve the topology of the triangulations (i.e. genus and orientation in two dimensions) and as such they are well-suited for generating large amounts of topological triangulations with a fixed genus. In order to be sure that we sample from all possible triangulations of genus g, we need to show the ergodicity of Pachner flips though. A rigorous proof of this only exists for point sets in two dimensions, however it has furthermore been shown that diagonal-edge flips are ergodic in the subset of triangulations with constant V for large enough V [51, 52]. When considering that insertion and removal Pachner flips can be used to "move" between subsets of triangulations with differing vertex number, we can (knowingly that this is not a strict proof) assume that Pachner flips are "ergodic enough" for our purpose.

5.2 Random Generation of Topological Triangulations

We will be concerned with the analysis of the Ising model in an random ensemble of topological triangulations. To this end, we present an algorithm to generate uniformly distributed triangulation samples. This algorithm is similar in concept to the one presented for lattice triangulations (cf. Section 4.1.3), however the lack of fixed geometry requires a few adjustments.

5.2.1 Construction via Pachner Flips

We want to generate uniformly distributed samples of triangulations with fixed genus g and vertex number V. The algorithm we use has essentially three steps: First, we construct a triangulation with the given genus without considering the vertex number. We then use the insertion and removal Pachner flips introduced in Section 5.1.2 to obtain a triangulation with the desired number of vertices. Finally, diagonal-edge flips are used to further randomize the triangulation. The output triangulation depends on the particular Pachner flips selected, hence executing this algorithm multiple times yields one sample triangulation per input random seed.

The construction of a triangulation with a particular genus g is trivial in the cases $g = 0$ and $g = 1$, for which we can start with any triangulation of the sphere and the torus, respectively. Since small systems are preferable due to computational costs, we pick the smallest possible triangulations for both the sphere and the torus, which have

four and seven vertices, respectively. For the sphere, such a triangulation has 4 vertices and the graph structure of a tetrahedron. For the torus, the minimal triangulation has 7 vertices and a nontrivial structure (see [53] for a concrete realization). For larger genera, we can use the classification theorem of closed surfaces, which states that any oriented topological surface is either the sphere or the connected sum of g tori[22]. In the other cases, the classification theorem becomes a *construction theorem* for our purpose: Given two (not necessarily different) particular triangulations of the torus manifold, a merged triangulation can be constructed by picking one triangle in each input triangulation and identifying the corresponding subsimplices of the triangles in a pairwise manner, which can be thought of as "glueing" the triangulations together at exactly one face. The result of this merger is a triangulation with 11 vertices[23] that is topologically equivalent to the connected sum of two tori, and hence has the genus $g = 2$. By repeating this process successively, we can increase the triangulation genus until the desired one is reached.

The constructed triangulation will in general have a different number of vertices than desired. We can use Pachner flips to insert or remove any number of vertices until the proper number V is reached, though. If V is larger than the vertex count in the constructed triangulation, we randomly select a triangle of the current triangulation and apply the corresponding insertion Pachner flip[24], which will in effect increase the number of vertices by one. This is repeated until the triangulation has the proper number of vertices. Similarly, if the amount of vertices in the constructed triangulation is greater than desired, we randomly select a vertex and use the corresponding removal Pachner flips to reduce the vertex count by one. Since in the latter case we may reach a triangulation for which there is no vertex with three incident edges (i.e. any further vertex removal would destroy the triangulation), we instead perform a diagonal-edge flip whenever an invalid removal flip was selected. Note that even with this strategy, the algorithm may converge slowly (or not terminate at all) since only few (or none) triangulations with the given genus and vertex number may actually exist.

Finally, the triangulation is further randomized by randomly selecting an edge of the triangulation and applying the corresponding diagonal-edge Pachner flip if possible. The lack of fixed geometry implies that to fulfill detailed balance, a non-trivial acceptance probability needs to be used: One thing to consider is that inserting a vertex will form new (higher-dimensional) simplices and removing a vertex will remove all simplices that contained this vertex. In both cases, the change in the number of simplices incurs a change in the probability for selecting a particular simplex[25]. Furthermore, technically

[22] Note that the outlined procedure can be generalized to non-oriented surfaces by use of triangulations of projective planes.

[23] It has twice the amount of vertices of a single minimal torus triangulation minus three vertices which have been identified with others in the merger.

[24] There is an acceptance probability assigned to the execution of this flip, similar to the diagonal-edge flips as used for lattice triangulations. However even though we are are only concerned with random triangulations in this section, this probability is not 1 as before because the selection probability before and after the flip will be different (see below), such that the detailed balance condition (2.17) requires the acceptance probability to be adjusted accordingly.

[25] For instance, when selecting a random 1-simplex (i.e. an edge) in a triangulation which has six 1-simplices in total, each 1-simplex has a chance of $\frac{1}{6}$ to be selected. When inserting a new vertex

different Pachner flips may lead to isomophic triangulations (the abstract simplicial complexes of which are equivalent up to permutations). Checking for such equivalences becomes very costly for large systems. This is only an issue issue for triangulations with particular symmetries though, and it has been shown that the number of these triangulations is negligible for triangulations with more than 30 triangles [54]. We hence omit the permutation equivalence check for systems with 64 or more vertices. Considering these effects in the selection probability, we roll and (if possible) apply 10000 diagonal-edge flips, after which the algorithm is finished and repeated to sample the next triangulation.

5.2.2 Minimal System Size for given Genera

We are interested in comparing triangulations of varying size against each other to see how system size affects system behavior. For this purpose, it is best to start with minimal triangulations, i.e. those that minimize vertex number at a fixed genus, and gradually increase system size from there. The minimal vertex number clearly is not arbitrarily small, since a certain number is required to encode all topologically relevant information. In fact, there is a tight lower bound for this minimal number of vertices which is based on the Heawood conjecture [55] from the context of graph coloring as cited by [56]. The conjecture was proven by Jungermann and Ringel [57] for orientable triangulations and by Ringel [58] for nonorientable ones. The bound is given by

$$\binom{v-3}{2} \geq 3 \cdot (2-\chi). \tag{5.7}$$

This implies that the vertex count of minimal triangulations of orientable manifolds is given by

$$v_{\min}(g) = \left\lceil \frac{7}{2} + \frac{1}{2}\sqrt{1+48g} \right\rceil. \tag{5.8}$$

In contrast, the triangulations constructed to initialize the algorithm explained in Section 5.2.1 are in general much larger[26] than minimal triangulations. We can reduce the triangulation size using removal Pachner flips (see above), but since the number of minimal triangulations may be much smaller than the total configuration space, our algorithm may not converge in reasonable time and hence it is not a priori clear how close our smallest generated triangulations are to being minimal.

Comparing our generated triangulations against the Heawood-bound, we see that for small triangulation genera ($g < 15$), our method yields almost minimal triangulations matching the Heawood-bound, while for genera beyond that there is an increasing deviation from the predicted minimal vertex count. For $g = 700$, we generate a triangulation with 208 vertices compared to the minimal number 96. The bounds are compared in Figure 21 for different values of g.

using a Pachner flip, the new triangulation has three additional 1-simplices, and the probability for each edge to be picked is $\frac{1}{8}$.

[26] Their size is $7 + 4g$ vertices for $g \geq 0$, corresponding to the size of the torus triangulation plus the number of vertices added for each torus that is "appended" by a connected sum.

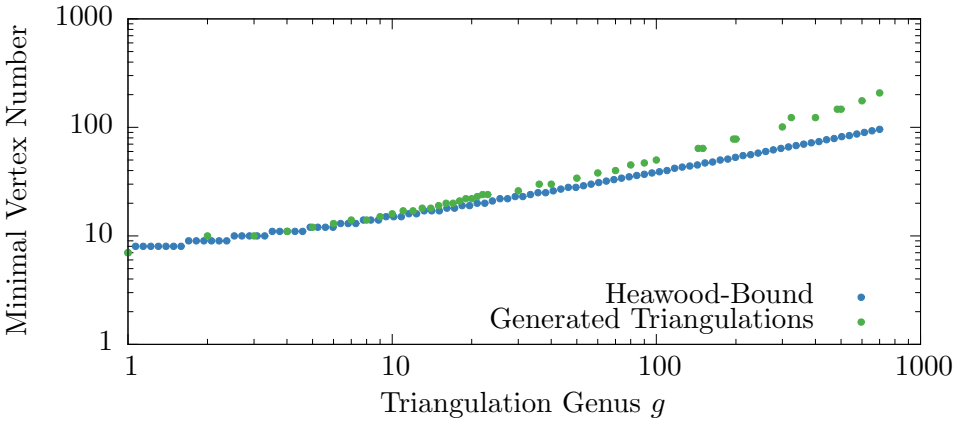

Figure 21: Vertex number of minimal triangulations for different genera compared to the smallest triangulation generated by our algorithm: For small triangulation genera, our algorithm produces triangulations that are reasonably close to being minimal, while more complex triangulations ($g = 700$) are 2.2 times as large as the minimal bound.

5.3 Critical Ising-Temperature

We now analyze the critical temperature of the phase transition in the Ising model on a quenched random ensemble of topological triangulations, i.e. we will analyze the model on each realized triangulation individually and then average the observed results over the triangulation ensemble. We generate the random ensemble using Pachner flips according to Section 5.2.1. Similar to Section 4.2, our analysis is based on the density of Ising states obtained for each triangulation individually using the Wang-Landau algorithm. Due to problems that we encountered, we are not able to make any judgements on critical exponents and our analysis is limited to the critical temperature of the phase transition.

Our initial approach to obtain the critical temperature was applying Binder cumulant analysis methods explained in Section 3.2.2, however we faced similar issues as in Sections 4.2.3 and 4.2.4: The sampled triangulations may be very diverse, hence comparing across system sizes yields very diverse and erroneous results. As a consequence, we instead determine the critical temperature from the maximum of the magnetic susceptibility χ. This method is affected more strongly by finite-size effects, however compared to lattice triangulations we have access to much larger systems since the computational cost of computing the density of Ising states is far more manageable due to the lack of open boundaries.

Using this method, we first compute critical temperatures for a selected set of genera ($g \in \{0, 1, 10, 100\}$) and for different system sizes ranging from 4 through 1024 vertices. The results are given in Figure 22. We can see that all graphs converge towards a fixed value, albeit this is debatable for the extremely erroneous $g = 100$ case. Considering the slope of each curve, the $g = 0$ case decreases monotonically with system size while $g >= 10$ cases increase monotonically (and the curve slope furthermore scales with the

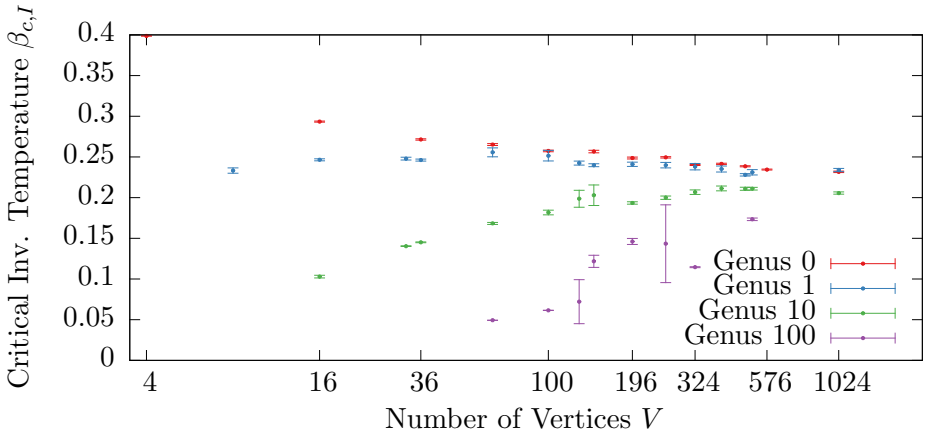

Figure 22: Dependence of critical Ising-temperature on the system size V, plotted for various genera. Denoted errors are standard deviations measured from 100 triangulations of each system size and genus.

genus since the $g = 100$ curve is much steeper than the $g = 10$ one). For a genus of 1, there is no major dependence on the system size.

We can explain this behavior using the following considerations: For triangulations of oriented surfaces with Euler characteristic $\chi = 2-2g$, v vertices, e edges, and t triangles, we know that

$$\chi = 2 - 2g = v - e + t. \tag{5.9}$$

We furthermore know that each triangle is constituted by three edges, each of which is shared by another triangle, and hence $2e = 3t$. Putting this into Equation (5.9) and rewriting it yields

$$\frac{e}{v} = 3 + \frac{6g - 6}{v}, \tag{5.10}$$

i.e. the ratio of edges to vertices is the sum of a constant (which is the same value of the ratio of lattice triangulations in the $N \to \infty$ limit) and a term linear in the genus and reciprocal in the number of vertices. Assuming a law analogous to the analytic expression in Equation (3.16) for the critical temperature in the square lattice Ising model holds, the inverse critical temperature $\beta_{c,I}$ scales reciprocally with the coupling constant. Since the ratio of edges to vertices is effectively increased, we can consider an effective coupling constant that is bigger by the same factor. This explains most observed effects: For fixed genus and large number of vertices the second term on the right-hand side of Equation (5.10) vanishes and the ratio converges towards the genus-independent value 3. Furthermore, in the small-system regime the genus determines the slope, which in particular means the $g = 0$ and $g \geq 2$ case have negative and positive slope, respectively, while $g = 1$ shows little to no dependence on the system size.

Assuming Equation (5.10) to hold at least approximatively provides for a good way to estimate the infinite-system limit of the critical temperature: Since $\frac{e}{v}$ is expected to be proportional to some effective coupling constant which in turn is reciprocal to the

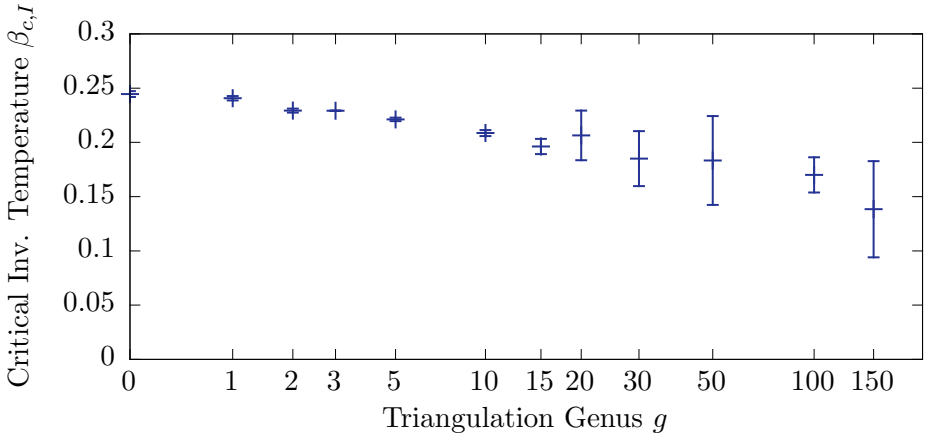

Figure 23: Critical Ising-temperature by genus, determined by fitting Equation (5.11) for each genus against data gathered from 100 triangulations each considered system size. Denoted are fit errors of the Marquardt-Levenberg algorithm used by gnuplot.

critical temperature, the equation translates to the relation

$$\beta_{c,I}{}^{V}(g) = a \cdot g^{-1} + \beta_{c,I}{}^{\infty}(g) \tag{5.11}$$

between the finite-size estimations $\beta_{c,I}{}^{V}(g)$ and the infinite-system limit $\beta_{c,I}{}^{\infty}(g)$. We perform a fit on this relation for fixed genus and different system sizes, and show the gathered results in Figure 23. The graph suggests that there is a monotonous decrease of the inverse critical temperature with the triangulation genus. However, results also have an increasingly large error which reduces the conclusiveness of our results. Since we looked at a fairly small number of triangulations (100 realizations per genus and system size), a larger set of data points may be helpful to improve the significance. However, since triangulations with larger genus have a much larger minimal size, a better approach might be to instead focus gathering data for larger system sizes.

6 Outlook

In the first part of this thesis, the properties of the Ising model on lattice triangulations were analyzed. While we have successfully described the critical behavior of the perfectly ordered lattice triangulation, our estimates of the critical exponents of realizations of random triangulation ensembles are scattered distributions. This result is unexpected from the theory of phase transitions, which predicts similar systems to exhibit critical exponents in the same universality class. This discrepancy may be due to our approach of comparing two possibly very different triangulations against each other to obtain the critical temperature from Binder cumulant considerations. We might be averaging two (or more) different subsets of triangulations of particular universality classes such that instead of well-defined maxima we obtain a single smeared distribution of exponents. Hence it would be interesting to see how other methods compare to our results. For instance, a finite-size scaling ansatz might be sufficient to obtain useful estimates even on small lattices if finite-size effects are considered by corrections to the FSS laws.

For canonical ensembles of lattice triangulations, we were severely limited by finite-size effects. This became apparent when we tried to determine critical exponents based on triangulations of a 10×10 lattice and couldn't get any useful information out of the data whatsoever (cf. Figure 18). It may be possible to improve the results by including finite-size corrections, however even then the system size is very restrictive. The main issue stopping us from considering larger systems is the computational effort required to compute the density of states with regards to the order measure (4.3) using the Wang-Landau algorithm. However, as described in [13], it is possible to compute the density of states for up to 24×24 lattices by introducing energy cutoffs similar to the one we introduced in Section 2.3.2. This is because in the regimes of lowest and highest energy, high entropy differences between the energy levels that are connected by diagonal-edge flips result in long runtimes of the Wang-Landau algorithm. However, introducing such cutoffs also prevents analysis of triangulations within the ignored energy regimes. A cutoff for high energies hence prevents accurate analysis of unordered triangulations ($\alpha < 0$), but might allow for better analysis of the transition region from random triangulations ($\alpha = 0$) to the perfectly ordered triangulation ($\alpha = \infty$). Furthermore, adding a second cutoff at lower energies might allow for the close vicinity of $\alpha = 0$ to be analyzed in detail.

Regardless of these issues encountered, we can provide a summary of results we expect to hold: In Figure 17, we have seen that there is a cross-over behavior in the Ising phase transition temperature between disordered and ordered lattice triangulations. We suspect such a cross-over behavior to occur for the critical exponents, too. In particular, all ordered triangulations ($\alpha > \epsilon_+$ for some $\epsilon_+ > 0$) will likely be in the universality class of the perfectly ordered triangulation, which is the standard 2D universality class, while disordered triangulations ($\alpha < \epsilon_-$ for $\epsilon_- < 0$) might be interconnected heavily enough to be part of the mean field universality class. If these two regimes indeed manifest, it would be interesting to analyze the critical behavior of the transition region $\epsilon_- < \alpha < \epsilon_+$.

The second part of the thesis was concerned with topological triangulations. Unfortunately, similar issues to the random lattice triangulation ensemble were encountered,

because the triangulations of fixed genus and vertex size may look vastly different. In fact, initial analysis using Binder cumulant methods yielded no conclusive results at all, which is why we had to employ finite-size scaling ansätze throughout the whole analysis. We have not yet been able to look into critical exponents, but we expect two limit cases to hold: When the system is large (with regards to the number of vertices of the triangulation) compared to the minimal triangulation with the given genus g, the local neighborhood of every vertex is approximately two-dimensional, which suggests that the critical exponents in this case match those of the 2D Ising model. On the other hand, for vertex numbers that are close to those of the minimal triangulation, the graph induced by the triangulation behaves more like a complicated object in three or more dimensions. As such, we expect this case to have critical exponents of a different universality class — possibly the one of 3D Ising model or of mean-field theory.

References

[1]E. Ising, "Beitrag zur Theorie des Ferromagnetismus", Z. Phys. **31**, 253–258 (1925).

[2]L. Onsager, "Crystal statistics. i. a two-dimensional model with an order-disorder transition", Phys. Rev. **65**, 117–149 (1944).

[3]S. M. Bhattacharjee and A. Khare, "Fifty years of the exact solution of the two-dimensional Ising model by Onsager", Curr. Sci. **69**, 816–821 (1995).

[4]A. Barrat and M. Weigt, "On the properties of small-world network models", EPJ B **13**, 547–560 (2000).

[5]M. Gitterman, "Small-world phenomena in physics: the Ising model", J. Phys. A **33**, 8373 (2000).

[6]H Hong, B. J. Kim, and M. Choi, "Comment on Ising model on a small world networki", Phys Rev E Stat Nonlin Soft Matter Phys **66**, 018101 (2002).

[7]A. Aleksiejuk, J. A. Hołyst, and D. Stauffer, "Ferromagnetic phase transition in Barabási–Albert networks", Physica A **310**, 260–266 (2002).

[8]H. Edelsbrunner, "Triangulations and meshes in computational geometry", Acta Numer. **9**, 133–213 (2000).

[9]C. Rovelli, *Quantum gravity* (Cambridge university press, 2007).

[10]J. Ambjørn, "Quantum gravity represented as dynamical triangulations", Class. Quantum Grav. **12**, 2079 (1995).

[11]J. Ambjørn, J. Jurkiewicz, and R. Loll, "Reconstructing the universe", Phys. Rev. D **72**, 064014 (2005).

[12]B. Krüger, E. M. Schmidt, and K. Mecke, "Unimodular lattice triangulations as small-world and scale-free random graphs", New J. Phys. **17**, 023013 (2015).

[13]J. F. Knauf, B. Krüger, and K. Mecke, "Entropy of unimodular lattice triangulations", Europhys. Lett. **109**, 40011 (2015).

[14]T. Aste, R. Gramatica, and T Di Matteo, "Exploring complex networks via topological embedding on surfaces", Phys. Rev. E **86**, 036109 (2012).

[15]T. Zhou, G. Yan, and B.-H. Wang, "Maximal planar networks with large clustering coefficient and power-law degree distribution", Phys. Rev. E **71**, 046141 (2005).

[16]D. Chandler, *Introduction to modern statistical mechanics* (Oxford University Press, 1987).

[17]C. Garrod, *Statistical mechanics and thermodynamics*, Vol. 1 (Oxford University Press, 1995).

[18]H. Gould and J. Tobochnik, *Statistical and thermal physics: with computer applications* (Princeton University Press, 2010).

[19]F. Reif, *Fundamentals of statistical and thermal physics* (Waveland Press, 2009).

[20]G. Jaeger, "The Ehrenfest classification of phase transitions: introduction and evolution", Arch. Hist. Exact Sci. **53**, 51–81 (1998).

[21]K. G. Wilson, "Renormalisation group and Kadanoff scaling picture", Physics Rev. B **4**, 3174 (1971).

[22]D. W. Heermann and K. Binder, *Monte carlo simulation in statistical physics* (Springer, Berlin Heidelberg, 2010).

[23]D. P. Landau and K. Binder, *A guide to monte carlo simulations in statistical physics* (Cambridge University Press, 2014).

[24]J. Moshman, "Random number generation", in *Mathematical methods for digital computers*, Vol. 2 (John Wiley New York, 1967), pp. 249–263.

[25]G. T. Barkema and M. E. J. Newman, *Monte carlo methods in statistical physics* (Oxford University Press, 2001).

[26]F. Wang and D. Landau, "Determining the density of states for classical statistical models: a random walk algorithm to produce a flat histogram", Phys Rev E Stat Nonlin Soft Matter Phys **64**, 056101 (2001).

[27]H. A. Bethe, "Statistical theory of superlattices", Proc. R. Soc. A **150**, 552–575 (1935).

[28]R. E. Peierls, "On Ising's ferromagnet model", **32**, 477–481 (1936).

[29]S. N. Dorogovtsev, A. V. Goltsev, and J. F. Mendes, "Critical phenomena in complex networks", Rev. Mod. Phys. **80**, 1275 (2008).

[30]M. Megard, G. Parisi, and M. A. Virasoo, "Spin glass theory and beyond", (1987).

[31]W. Janke, "Monte carlo simulations of spin systems", in *Computational physics* (Springer, 1996), pp. 10–43.

[32]M. Fisher, "The theory of critical point singularities", Critical phenomena, 1–99 (1971).

[33]V. Privman, ed., *Finite size scaling and numerical simulation of statistical systems* (World Scientific, Singapore, 1990).

[34]K. Binder, "Finite size scaling analysis of Ising model block distribution functions", Zeitschrift für Physik B Condensed Matter **43**, 119–140 (1981).

[35]W. Selke and L. N. Shchur, "Critical Binder cumulant in a two-dimensional anisotropic Ising model with competing interactions", Phys Rev E Stat Nonlin Soft Matter Phys **80**, 042104 (2009).

[36]W. Selke and L. N. Shchur, "Critical binder cumulant in two-dimensional anisotropic Ising models", J. Phys. A **38**, L739 (2005).

[37]R. J. Baxter, *Exactly solved models in statistical mechanics* (Courier Corporation, 2007).

[38]G. Benettin, G. Gallavotti, G. Jona-Lasinio, and A. L. Stella, "On the Onsager-Yang-value of the spontaneous magnetization", Communications in Mathematical Physics **30**, 45–54 (1973).

[39]A. Pelissetto and E. Vicari, "Critical phenomena and renormalization-group theory", Phys. Rep. **368**, 549–727 (2002).

[40]M. Campostrini, A. Pelissetto, P. Rossi, and E. Vicari, "25th-order high-temperature expansion results for three-dimensional Ising-like systems on the simple-cubic lattice", Phys. Rev. E **65**, 066127 (2002).

[41]S. N. Dorogovtsev, A. V. Goltsev, and J. F. F. Mendes, "Ising model on networks with an arbitrary distribution of connections", Phys Rev E Stat Nonlin Soft Matter Phys **66**, 016104 (2002).

[42]M. Leone, A. Vázquez, A. Vespignani, and R. Zecchina, "Ferromagnetic ordering in graphs with arbitrary degree distribution", EPJ B **28**, 191–197 (2002).

[43]S. Dommers, C. Giardinà, and R. van der Hofstad, "Ising critical exponents on random trees and graphs", Commun. Math. Phys. **328**, 355–395 (2014).

[44]V. Kaibel and G. M. Ziegler, "Counting lattice triangulations", in *Surveys in combinatorics*, Vol. 307 (Cambridge Univ. Press Cambridge, 2003), pp. 277–307.

[45]U. von Pachner, "Konstruktionsmethoden und das kombinatorische Homöomorphieproblem für Triangulationen kompakter semilinearer Mannigfaltigkeiten", in Abhandlungen aus dem Mathematischen Seminar der Universität Hamburg, Vol. 57, 1 (Springer, 1987), pp. 69–86.

[46]J. De Loera, J Rambau, and F Santos, *Triangulations: applications, structures and algorithms. number 25 in algorithms and computation in mathematics*, Heidelberg, 2010.

[47]C. L. Lawson, "Transforming triangulations", Discrete mathematics **3**, 365–372 (1972).

[48]R. Oeckl, *Discrete gauge theory: from lattices to TQFT* (Imperial College Press, 2005).

[49]R. Fritsch and R. Piccinini, *Cellular structures in topology* (Cambridge University press, 1990).

[50]B. Krüger and K. Mecke, "Genus dependence of the number of (non-)orientable surface triangulations", unpublished, 2015.

[51]S. Negami, "Diagonal flips in triangulations of surfaces", Discrete Math. **135**, 225–232 (1994).

[52]S. A. King, "Regular flip equivalence of surface triangulations", Topol. Appl. **127**, 169–173 (2003).

[53]A. Császár, "A polyhedron without diagonals", Acta Sci. Math. **13**, 140–142 (1949–1950).

[54]L. B. Richmond and N. C. Wormald, "Almost all maps are asymmetric", J. Comb. Theory B **63**, 1–7 (1995).

[55]H. Percy John, "Map-colour theorem", Quart. J. Pure Appl. Math. **24**, 332–338 (1890).

[56]F. H. Lutz, "Triangulated manifolds with few vertices: combinatorial manifolds", arXiv: math/0506372 (2005).

[57]M. Jungerman and G. Ringel, "Minimal triangulations on orientable surfaces", Acta Math. **145**, 121–154 (1980).

[58]G. Ringel, "Wie man die geschlossenen nichtorientierbaren Flächen in möglichst wenig Dreiecke zerlegen kann", Math. Ann. **130**, 317–326 (1955).

Erklärung

Ich versichere, dass ich meine Masterarbeit ohne Hilfe Dritter und ohne Benutzung anderer als der angegebenen Quellen und Hilfsmittel angefertigt habe und die aus benutzten Quellen wörtlich oder inhaltlich entnommenen Stellen als solche kenntlich gemacht habe. Diese Arbeit hat in gleicher oder ähnlicher Form noch keiner Prüfungsbehörde vorgelegen.

Erlangen, den 15. Januar 2016 Tony Wasserka